

Dissertation

Generation and applications of controlled waveforms from a laser oscillator

ausgeführt zum Zwecke der Erlangung des akademischen Grades eines
Doktors der technischen Wissenschaften unter der Leitung von

Univ.-Prof. Dr. Ferenc Krausz
Institut für Photonik, E387

eingereicht an der Technischen Universität Wien
Fakultät für Elektrotechnik und Informationstechnik
von

Mag. rer. nat. Péter Dombi

0127153

1060 Wien, Gfrornergasse 3/1/29

Wien, im Jänner 2005

Kurzfassung

Erzeugung und Anwendungen gesteuerter Wellenformen aus einem Laseroszillator

Es gibt viele Methoden, wie man eine elektromagnetische Wellenform im Hochfrequenzbereich steuert. Sogar für Terahertz-Pulse (die den spektralen Bereich zwischen optischen Frequenzen und Mikrowellen überbrücken) kann man eine bestimmte zeitliche Entwicklung des elektrischen Feldes verwirklichen. Dennoch war mit den üblichen Methoden für optische Pulse bis vor kurzem nur der Zugang zur Form der Einhüllende des Pulses ermöglicht.

Zum ersten Mal wurde die relative Phase zwischen der Trägerwelle und der Einhüllende (sog. carrier-envelope (CE) Phase) eines optischen Pulses im Jahr 2000 stabilisiert. Weitere Schritte mussten gemacht werden, um dieses Verfahren sowohl bezüglich der Lasertechnologie, als auch bezüglich der Grundforschungsperspektive ausschöpfen zu können. Meine Dissertation enthält Beiträge zu beiden Bereichen. Einerseits muss die Lasertechnologie verbessert werden, um immer kürzere Pulse mit gewünschter Einhüllende und Trägerwelle liefern zu können. Andererseits muss man zu einem besseren Verständnis der Rolle der CE-Phase bei Licht-Materie-Wechselwirkungsprozessen kommen. Vor kurzem stellte sich auch experimentell heraus, dass die gesteuerte Erzeugung optischer Wellenformen bei reproduzierbarer Herstellung isolierter Attosekundenpulse erforderlich ist und verdient daher in der Zukunft nähere Aufmerksamkeit, auch deswegen weil es bei den aktuellen Verfahren der CE-Phasenstabilisierung noch viel zu verbessern gibt. Überdies können viele grundlegende physikalische Phänomene ein neues Gesicht zeigen, wenn die üblichen Licht-Materie-Wechselwirkungsprozesse durch „gesteuerte Wellenform-Materie-Wechselwirkungen“ ersetzt werden. Meine Beiträge sind wie folgt:

- 1.) Basierend auf einem existierenden Ti:Saphir Oszillator mit einem langen Resonator und einem sog. f - $2f$ Interferometer (und Elektronik) für die Stabilisierung der CE-Phase, baute ich – meines Wissens nach – das erste CE-Phasenstabilisierte Lasersystem, in dem nur ein kleiner Anteil (15%) des optischen Outputs war angewendet, um die CE-Phase stabilisierende Regelschleife zu schließen. Demnach konnte der Großteil des Strahles wirksam in einem Beamline genutzt werden, wobei die Pulskompression auf eine sub-4-fs Dauer ausgeführt wurde, um Licht-Materie-Wechselwirkungsexperimente mit gesteuerten optischen Wellenformen zum ersten

Mal verwirklichen zu können, deren Länge nur das 1.5-fache des optischen Zyklus beträgt. Außerdem war ein Nebengewinn dieser Anstrengungen die Charakterisierung und Rekonstruktion der zeitlichen Entwicklung eines sub-4-fs Laserpulses mit einem einfachen Autokorrelator (angepasst auf diese außerordentlich kurze Pulsdauer), die damals die kürzesten optischen Pulse waren. Zusätzlich wurde ein neuer nichtlinearer Effekt bei der Ausbreitung ultrakurzer Pulspaare in einer mikrostrukturierten Faser entdeckt. (V. S. Yakovlev, P. Dombi et al., *Appl. Phys. B*, **76**, 329 (2003) und V. L. Kalashnikov, P. Dombi et al., *Appl. Phys. B*, **77**, 319 (2003)).

2.) Auf dem oben beschriebenen Lasersystem basierend zeigte ich, dass die Elektronenausbeute der multiphotoneninduzierte Oberflächen-Photoelektronemission (multi-photon-induced surface photoelectron emission, MSPE) unmittelbar empfindlich auf die CE-Phase ist. Dies war die erste Beobachtung eines physikalischen Prozesses in einem Festkörper, der nicht nur durch die Einhüllende des Laserpulses unmittelbar beeinflusst wurde, sondern auch durch die optische Wellenform. Im Gegensatz zu den üblichen CE-Phasenstabilisierungsverfahren, f - $2f$ Interferometrie, die nur von der Puls-zu-Puls Verschiebung der CE-Phase in einem modengekoppelten Pulszug abhängig ist, lieferte meine Messung unmittelbare Informationen über die CE-Phase eines Einzelpulses in einem Pulszug. Ich führte zeitaufgelöste MSPE-Messungen aus, um die von den Erwartungen abweichende, niedrigere Abhängigkeit dieses Prozesses von der CE-Phase erklären zu können. (A. Apolonski, P. Dombi et al., *Phys. Rev. Lett.* **92**, 073902 (2004), P. Dombi et al., *New J. Phys.*, **6**, 39 (2004) und P. Dombi et al., in Vorbereitung (2005)).

3.) Ich führte lineare Analyse über CE-Phasenänderungen bei der Ausbreitung von Laserpuls durch, die nur wenige optische Zyklen enthalten, und wies darauf hin, dass in diesem Parameterbereich f - $2f$ Interferometrie (die üblicherweise für CE-Phasenstabilisierung verwendet wird) für die Kompensation allfälliger, außerhalb des Laseroszillators auftretenden CE-Phasenverschiebungen grundsätzlich nicht geeignet ist. Deswegen sollte unmittelbare Phasenmessung verwendet und aus einem solchen Verfahren stammendes Fehlersignal ins Lasersystem rückgekoppelt werden (z. B. auf MSPE-basierend), wenn man einen langen Pulszug mit identischen Wellenformen auf dem Target braucht. So dient diese Analyse als Basis für „on-target“ Phasenstabilisierung. (P. Dombi et al., *New J. Phys.*, **6**, 39 (2004)).

Relevante Publikationen

- [1] V. S. Yakovlev, **P. Dombi**, G. Tempea, C. Lemell, J. Burgdörfer, T. Udem, A. Apolonski, “Phase-stabilized 4-fs pulses at the full oscillator repetition rate for a photoemission experiment”, *Appl. Phys. B* **76**, 329-332 (2003).
- [2] V. L. Kalashnikov, **P. Dombi**, T. Fuji, W. J. Wadsworth, J. C. Knight, P. S. J. Russell, R. S. Windeler, A. Apolonski, “Maximization of supercontinua in photonic crystal fibers by using double pulses and polarization effects” *Appl. Phys. B* **77**, 319-324 (2003).
- [3] **P. Dombi**, A. Apolonski, G. G. Paulus, M. Kakehata, R. Holzwarth, Th. Udem, Ch. Lemell, J. Burgdörfer, T. W. Hänsch and F. Krausz, “Solid-state light phase detector” CLEO/QELS, Baltimore, Maryland, USA, Postdeadline paper QThPDA4 (2003).
- [4] **P. Dombi**, A. Apolonski, G. G. Paulus, M. Kakehata, R. Holzwarth, Th. Udem, Ch. Lemell, J. Burgdörfer, T. W. Hänsch and F. Krausz, “Lichtphasendetektor aus Festkörper” 53. Jahrestagung der Österreichischen Physikalischen Gesellschaft, Salzburg, Austria, Beitrag F-QEO03 (2003).
- [5] A. Apolonski, **P. Dombi**, G. G. Paulus, M. Kakehata, R. Holzwarth, Th. Udem, Ch. Lemell, K. Torizuka, J. Burgdörfer, T. W. Hänsch, F. Krausz, „Observation of light-phase-sensitive photoemission from a metal“ *Phys. Rev. Lett.* **92**, 073902 (2004).
- [6] **P. Dombi**, A. Apolonski, Ch. Lemell, G.G. Paulus, M. Kakehata, R. Holzwarth, Th. Udem, K. Torizuka, J. Burgdörfer, T. W. Hänsch, F. Krausz, „Direct measurement and analysis of the carrier-envelope phase in light pulses approaching the single-cycle regime“, *New J. Phys.* **6**, 39 (2004).
- [7] **P. Dombi**, A. Apolonski, G. G. Paulus, M. Kakehata, R. Holzwarth, Th. Udem, Ch. Lemell, J. Burgdörfer, T. W. Hänsch and F. Krausz, “Solid-state carrier-envelope phase detector” Ultrafast Optics IV Proceedings, p. 185-191, Springer Verlag (2004).
- [8] **P. Dombi**, A. Apolonski, F. Krausz, “Photoelectrons measuring the phase of light” *EuroPhysics News*, Juli/August Ausgabe (2004), eingeladener Beitrag.
- [9] Ch. Lemell, **P. Dombi**, X.-M. Tong, F. Krausz, J. Burgdörfer, „Determination of the carrier-envelope phase of ultrashort laser pulses using metal surfaces” 68. Physikertagung der Deutschen Physikalischen Gesellschaft, München, Deutschland, Paper Q42.7 (2004).
- [10] **P. Dombi**, F. Krausz, Gy. Farkas, “Ultrafast dynamics of multiphoton photoemission and carrier-envelope phase sensitivity”, *Advanced Solid-State Photonics*, Wien, Österreich (2005), akzeptiert.
- [11] **P. Dombi**, F. Krausz, Gy. Farkas, “Ultrafast dynamics of multiphoton photoemission and carrier-envelope phase sensitivity”, in Vorbereitung (2005).

Contents

Kurzfassung	2
Relevante Publikationen	4
1 Motivation and objectives	6
2 Construction of a sub-4-fs, CE phase stabilized laser system	13
2.1 Principles and state-of-the-art of CE phase stabilization	13
2.2 Overview of the building blocks of the laser system	17
2.3 Pulse compression with TFI chirped mirrors and pulse envelope diagnostics	19
2.4 Out-of-loop CE phase diagnostics	24
3 Laser-solid interaction induced by controlled optical waveforms	28
3.1 Overview of light-matter interaction from the CE phase sensitivity point-of-view	28
3.2 Theoretical basis of CE phase sensitivity of multi-photon photoemission	32
3.3 Multi-photon photoemission experiments with controlled optical waveforms	37
3.4 Diagnostic and time-resolved measurements of multi-photon photoemission with few-cycle pulses.....	44
3.5 Discussion and outlook	49
4 Analysis of CE phase effects upon ultrashort pulse propagation	51
4.1 Few-cycle pulse propagation and interactions	51
4.2 Drawbacks of f-to-2f interferometry	53
4.3 Effects of linear pulse propagation on the CE phase	55
4.4 Direct CE phase stabilization	56
5 Conclusions and outlook	60
Abbreviations	62
Bibliography	63
Full publication list of the author	67
Lebenslauf	69

1 Motivation and objectives

Manipulating electromagnetic oscillations is a basic task of applied science. As to which fields of science are involved depends on the spectral region concerned, but the question arises in most branches of electronics, optics etc. Most applications in terms of controlling waveforms (as opposed to controlling only pulse envelopes) had been limited to longer-wavelength domains, mainly, of course, to the radiofrequency domain, but even for THz pulses (which are spectrally bridging the gap between the microwave and the optical domain and have been investigated intensively in the past fifteen years, see Mittleman et al., 1996) one could recently realize a controlled temporal evolution of the electric field strength.

It is a sharp contrast that standard techniques for infrared and visible optical pulses (and also spectrally beyond, towards X-rays) until even very recently had been limited to gaining access to the shape of the envelope of the pulse only. Typical research areas, where pulse shaping techniques had become standard tools include femtochemistry and coherent control experiments in the nineties (Zewail, 2000). Laser pulses with controlled envelopes brought immense success to selectively breaking a chemical bond in a molecule (the related field is termed as site-selective photochemistry) or time-resolved studies of typical femtochemical and electron transport processes in solids, with pump-probe spectroscopy being the typical tool to carry out these investigations.

The actual phase of the carrier wave oscillations with respect to the (maximum) of the envelope of the laser pulse (the so-called carrier-envelope (CE) phase – sometimes also termed as the “absolute” phase with a certain degree of inaccuracy; see Fig. 1) can be quantified by φ , if one decomposes the electric field evolution in the form

$$E(t) = A(t)\cos(\omega_L t + \varphi) \quad (1)$$

into an envelope function $A(t)$ and the carrier wave with central laser frequency ω_L .

In the above-described interactions φ did not play a role. The reason for this is that these fundamental processes in nature have a typical timescale of 10-100 fs and compact ultrafast sources based on novel solid-state laser materials (the most important of which turned out to be Ti-doped sapphire, Ti:S) have their lasing wavelengths in the red wing of the visible and in the near infrared domain. The

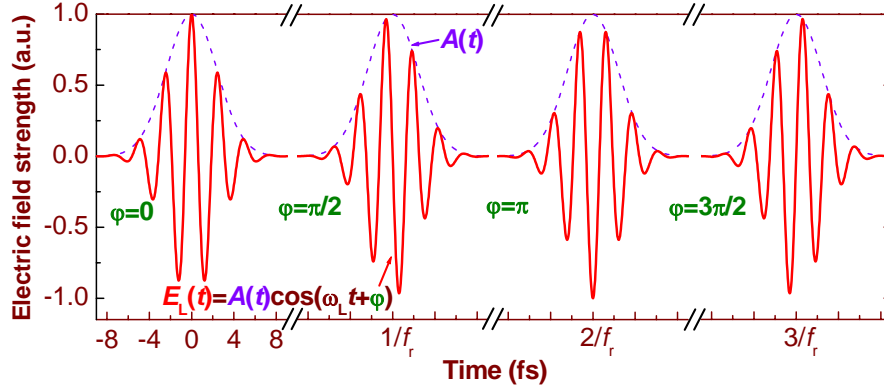


Figure 1. Different possible evolutions of the electric field $E_L(t)$ of few-cycle laser pulses having the same pulse envelope (pulse length, $\tau_p = 4$ fs, $\lambda_0 = 750$ nm, Gaussian pulse shape: $A(t) = A_0 \exp(-2t^2 \ln 2 / \tau_p^2)$, repetition rate: f_r). Once the envelope is fully characterized one needs only a single further parameter, the carrier-envelope phase (ϕ) to fully determine the electromagnetic waveform. The figure can also be regarded as the output pulse train of a mode-locked laser oscillator with the CE phase slipping from pulse to pulse with a certain amount ($\pi/2$ in the depicted case). In this case f_r is the repetition rate.

duration of an optical cycle of 800-nm-light (the Ti:S central wavelength) is 2.7 fs which is clearly below the typical timescale of processes in biological and chemical systems and most electron transport phenomena in solids can also be examined with 30-40 fs pulses that were readily available from these laser systems.

Even though 6-fs-pulses at around 600 nm were also generated at the end of the eighties the fact that this achievement relied on dye laser technology did not make it spread easily. It had to be with Ti:S lasers that a significant number of groups could shoot for sub-10-fs pulses with reasonably high pulse energies. With these pulses it was then possible to examine basic physical processes taking up unseen features as shorter and shorter pulses were applied. It was primarily at this time that questions were raised whether the well-known handling techniques of light-matter interaction and pump-probe spectroscopy were still applicable (Brabec and Krausz, 2000).

Two fundamental limitations were posed in terms of applying standard routines of these fields. The first is that the pulse length of Ti:S lasers started to become so short that it approached the period of the oscillation cycle. In this case the effect of potentially having different waveforms taking part in the interaction becomes a major concern, as one can imagine just by looking at Fig. 1. The second is that due to improvements in amplifier technology and pulse compression methods

unprecedented intensities could be reached with table-top systems. For example, when a laser pulse interacts with an atom and the electric field strength of the pulse becomes comparable to the binding atomic Coulomb-field of the most loosely bound electrons the standard perturbative handling of the interaction is not applicable any more. Perturbative interactions are typically governed by the pulse envelope, whereas in strong-field interactions the temporal evolution of the electric field strength plays a crucial role (for more details see Section 3.1). The next step in terms of increasing the intensity would be inducing relativistic interactions with the laser pulse where the magnetic field of the pulse also comes into play, but this parameter regime is not yet accessible with sub-10-fs sources, in spite of current technology being not far away from this point.

The fact that light-matter interaction could not be characterized any more by some oscillation with a quasiconstant amplitude in this parameter regime brought the necessity of getting rid of well-known and widely used approximations in the theoretical handling of these phenomena, such as the slowly varying envelope approximation and equations had to be solved in a more tedious manner. In time-resolved studies it also brought challenges since standard deconvolution methods using the independently characterized envelope of the interacting laser pulse are not sufficient any more. The breadth of new phenomena that are accessible in such a manner rewards copiously for these efforts. The most important of these new effects proved to be high harmonic generation (HHG) and I will use now this example to demonstrate basic concepts and benefits of few-cycle optical waveform control and applications.

High order harmonics are generated in a gaseous medium when a linearly polarized laser pulse of sufficient intensity interacts with atoms in a non-perturbative manner. The distortion of the atomic potential for the most loosely bound electrons by the laser field itself makes them able to tunnel out from the potential well. After this so-called “birth” of a free electron wavepacket (assumed to have zero initial velocity) its further motion is governed by the laser field only. Provided that this field is linearly polarized the electron wavepacket reaches the parent ion again after performing a wiggle in the laser field and recombines with it with a non-zero probability. The amount of energy released in this process typically in the form of extreme ultraviolet (XUV) photon emission is made up of two terms, the binding energy of the electron and the energy acquired by the free electron in the laser field.

This concrete phenomenon illustrates brilliantly how much the few-cycle nature of the pulses and the actual waveform can influence a strong-field interaction process. When HHG is induced by 30-40 fs pulses the XUV spectrum is made up of discrete odd-harmonic lines with quasi-constant amplitudes (the so-called plateau harmonics) and a cut-off region. The presence of plateau harmonics indicates the proper phase matching conditions only for discrete spectral lines and the lack of even order harmonics is due to the inversion symmetry of the medium they are generated in. Their quasi-constant amplitude is an indication of the non-perturbative nature of the interaction. The cut-off photon energy corresponds to the maximum energy that the wavepacket can acquire in the laser field.

It was foreseen and a couple of years ago also experimentally found (Schnürer et al., 1998) that applying few-cycle pulses to induce HHG changes drastically the nature of the process. The linewidths in the plateau region become larger due to the fact that the highest energy harmonics are generated only around the central, narrow part of the pulse having the highest electric field strength (Fig. 2, left-hand-side panel, blue curve). Without going into details at this point about techniques of waveform control it has to be mentioned that it was also observed that when

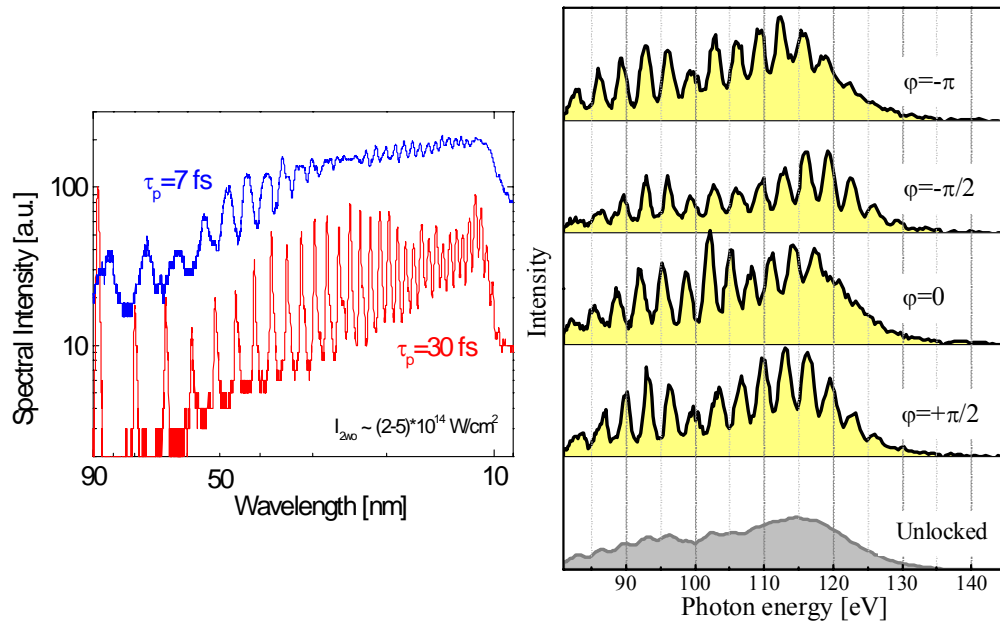


Figure 2. Spectrum of high harmonics generated with amplified Ti:sapphire laser pulses of different duration and waveform. For the results shown in the right-hand-side panel 5 fs pulses were used (adapted from Brabec and Krausz, 2000 and Baltuška et al., 2003)

harmonics are generated by a *sine* pulse ($\varphi = \pi/2$) the spectrum is completely different from that of a *cosine* pulse ($\varphi = 0$). For *cosine* pulses the spectrum smoothes out in the cut-off region and the plateau region does not contain strictly defined harmonics any more; the lines are now at different frequencies due to the few-cycle nature of the generating pulse (Fig. 2, right-hand-side panel).

Generation of attosecond pulses drew heavily on HHG. The idea that attosecond pulse trains could be synthesized from a series of high-harmonic lines in the plateau region (for example, similar to the red curve in Fig. 2) with mere Fourier-synthesis came more than a decade ago (Farkas and Tóth, 1992), well before technology was mature enough for experimental realization and proof. When it turned out that sub-10-fs pulses generate a much smoother HHG spectrum, researchers realized that this could form the basis of isolated attosecond pulse generation. Since these pulses were meant to be the shortest controllably producible physical effect in the world, it raised enormous attention when the first proof of the existence of isolated attosecond pulses were reported by Hentschel et al. in 2001. The potential yield of this step in basic research and time-resolved studies of the fastest processes mankind could ever take a look at cannot be overestimated.

Drawing on results illustrated in Fig. 2 the shortest attosecond XUV pulses have now a duration as short as 250 as and they are ideally generated by 5-fs-long, waveform-controlled *cosine*-pulses (Baltuška et al., 2003). It can be seen after the above motivations that development of proper technologies for controlled generation of these waveforms is of utmost importance for attosecond science* and I will give a detailed description of my contributions to waveform-control technologies later on in this thesis.

A desired device in terms of applications in attosecond science would be able to track accurately CE phase fluctuations of a chirped-pulse-amplified laser system

* It has to be mentioned here that independently of these vast benefits controlled optical waveforms can bring to attosecond science the first experimental realization of a CE phase controlled laser source (Jones et al., 2000) was carried out well before the final proof for isolated attosecond pulse generation (Hentschel et al., 2001) and even more time before the experimental demonstration of the effect of controlled optical waveforms on attosecond pulse generation (Baltuška et al., 2003). This means that considerations about and experiments with CE phase stabilized pulses were originally quite independent from attosecond science and were partly based on different motivations the most important of which is optical frequency metrology. These applications are also to be illuminated later in this thesis to some extent.

(typically used for attosecond pulse generation) using only a portion of the beam (preferably nJ pulse energies) on a single-shot basis. Once this information is fed back to the laser system almost perfect on-target CE phase stabilization can be provided. Another desired property of such a method would be that it relies only on laser-solid interaction, making it more compact and potentially avoiding expensive vacuum equipment.

In this thesis I will report on the first observation of CE phase sensitivity of multi-photon-induced surface photoelectron emission (MSPE) from a gold surface that is a potential candidate for fulfilling these criteria (Dombi et al., 2004). The development of a laser system that is capable of providing the necessary pulses for these investigations was also a challenging task and resulted in the first-ever laser in which only a portion of the beam was used for CE phase stabilization (with a method called f -to- $2f$ interferometry that is sensitive only to the pulse-to-pulse CE phase shift, but not its actual value) and so the major part of the output could be used for the photoelectron emission experiment (Yakovlev, Dombi et al., 2003). This was carried out with 4-fs laser pulses the generation and characterization of which was also part of my development work and these pulses were one of the shortest visible pulses ever generated at the time of these experiments.

The resulting proof I delivered for the CE phase sensitivity of MSPE was the first direct observation of a physical effect in a solid that was governed by the optical waveform of a laser pulse. Therefore MSPE is also capable of unambiguously delivering information on the CE phase value. There is a sharp contrast with the other method utilizing HHG developed simultaneously, relying on gas-phase strong-field interactions and showing a $\pm\pi$ ambiguity (Baltuška et al., 2003) in CE phase detection.

Once direct CE phase measurement is available the question can be asked whether it brings benefits by using it in a laser system that is already phase-stabilized with e.g. f -to- $2f$ interferometry. I provided a positive answer with a linear analysis of CE phase changes of few-cycle pulses upon propagation in a dispersive medium and pointed out for the first time that in this parameter regime f -to- $2f$ interferometry used as a standard CE phase stabilization method provides inadequate feedback signal for accurate stabilization (Dombi et al., 2004). Therefore, direct CE phase measurement (e.g. based on MSPE) has to be used and fed back if one needs a long train of optical pulses with identical waveforms on-target.

Practical implementation of such a scheme was, however, hindered by the low contrast of the effect observed, with the electron emission yield from the surface showing much less phase sensitivity than predicted by simulations. Therefore, I also carried out thorough diagnostic measurements with few-cycle laser pulses to check if the fundamental features of the emission process remain unchanged in this parameter regime. I also took a look at MSPE in a time-resolved manner yielding insights to the effect potentially reducing the CE phase contrast being identified as ultrafast electron dynamics upon the emission process (Dombi et al., 2005).

2 Construction of a sub-4-fs, CE phase stabilized laser system

The issue of CE phase stabilization of a laser oscillator was raised as early as 1996 by Xu et al. In the following four years several papers appeared about the potential significance of the CE phase in strong-field interactions and about the way it could be measured (Cormier and Lambropoulos, 1998, Reichert et al., 1999, Telle et al., 1999, Dietrich et al., 2000, Christov, 2000). In spite of the attention it raised, first realization of a CE phase stabilized laser system, however, was announced by two groups simultaneously only in 2000 (Diddams et al., 2000, Apolonski et al., 2000). This means that scientists at the turn of the millennium were equipped with only a handful of theoretical predictions and the laser (and electronics) technology. The link between potential new physics and CE phase stabilization technology was still missing. In this section I will describe the construction of a laser system that was able to bridge this gap for the first time in terms of laser-solid interactions.

2.1 Principles and state-of-the-art of CE phase stabilization

A free-running, mode-locked oscillator normally gives a pulse train in which the CE phase changes inherently by a certain (though significantly jittering) amount from one pulse to the other ($\Delta\phi$). Fig. 1 can be taken as an illustration for such a pulse train, too, with $\Delta\phi = \pi/4$. This phase shift from one pulse to its successor is rooted in the difference between the group and phase velocities within the cavity observed by the circulating pulse. In the spectral domain the pulse train forms a frequency comb with equidistant lines sitting under an envelope determined by the Fourier transform of a single pulse in the train (Fig. 3, upper panel, red curve and comb lines). The frequency of the n^{th} comb line can be written as

$$f_n = nf_r + f_{\text{ceo}} \quad (2)$$

where f_r is the repetition rate (and therefore also the amount by which the comb lines are separated) and f_{ceo} is the so-called carrier-envelope offset (CEO) frequency which gives the zero frequency offset of the frequency comb.

The CEO frequency can also be associated with the pulse-to-pulse rate of change of the CE phase in the pulse train ($\Delta\phi$) in the following form

$$\Delta\phi = 2\pi f_{\text{ceo}} / f_r \quad (3)$$

giving thus the link between the time-domain and frequency-domain pictures. Determining the CE phase evolution in the pulse train reduces therefore to determining f_{ceo} , which is a measurable quantity. Nevertheless its measurement is not trivial, since there is no signal at such low frequencies.

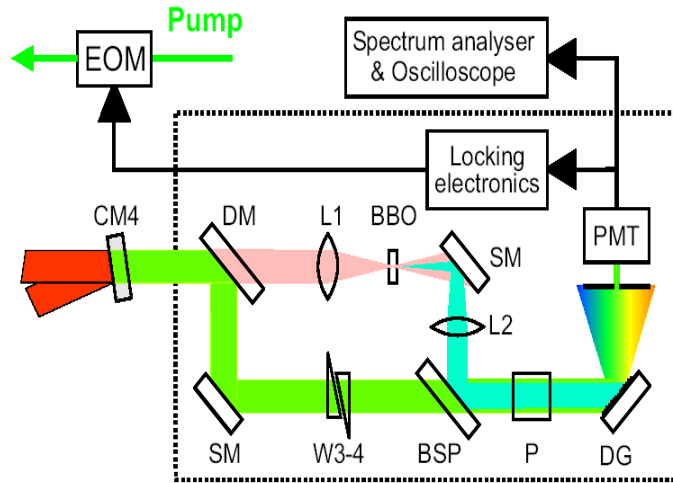
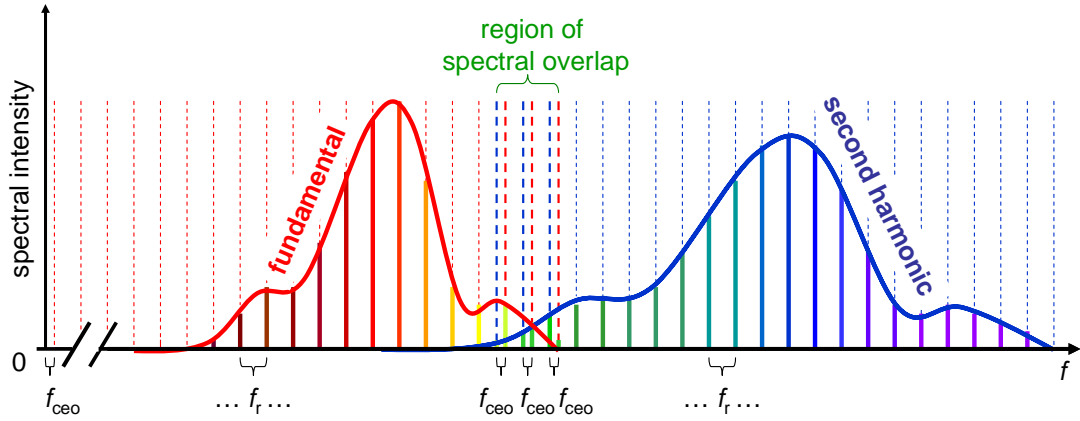


Figure 3. Upper panel: principle of f -to- $2f$ interferometry with the octave-spanning fundamental (red comb lines) and second harmonic (blue lines) frequency combs of the output of a mode-locked oscillator. If they overlap, the beat between these lines in the overlap region provides the zero frequency offset of the fundamental frequency comb. Lower panel: a potential implementation of the f -to- $2f$ method with a nonlinear Mach-Zehnder interferometer. DM: dichroic mirror, CM4: chirped mirror, SM: steering mirror, L1,L2: lenses, W3-4: wedge pair, BSP: beam splitter, P: polarizer, DG: diffraction grating, BBO: frequency doubling crystal (The lower panel is from Poppe et al., 2001.)

The ingenious idea behind the measurement of f_{ceo} is as follows (Reichert et al., 1999, Telle et al., 1999). If the frequency comb spans an octave and if the red wing of the comb can be frequency-doubled then the beating between the fundamental and second harmonic comb lines gives exactly f_{ceo} (as illustrated in the upper panel of Fig. 3) which can be checked with simple algebra. The comb lines in the fundamental frequency comb are given by equation (2). The generated second harmonic pulse train obviously has comb lines at $2(nf_r + f_{\text{ceo}})$. If there is an optical signal from the fundamental pulse train also at $2nf_r + f_{\text{ceo}}$ (it is here that the criterion of the octave-spanning fundamental bandwidth comes in) and if there are comb lines from the SH comb around this frequency (requiring broadband SHG) then the beat signal between the fundamental and the SH comb in this overlap region can be written as

$$2(nf_r + f_{\text{ceo}}) - (2nf_r + f_{\text{ceo}}) = f_{\text{ceo}} \quad (4)$$

giving exactly the CEO frequency that can be measured by spectrally filtering the overlap region and picking this rf beat with a photodiode.

Since the direct output of Kerr-lens mode-locked (KLM) Ti:S oscillators is far from octave-spanning the recently discovered photonic crystal fibres (PCFs, also called as microstructured fibres) are used to generate a supercontinuum with low energy pulses (Russell, 2003). The optical implementation of the further steps described in the previous paragraph take place mostly in a Mach-Zehnder-type interferometer that can also be seen in the lower panel of Fig. 3. Once the output of the interferometer is spectrally filtered the beat signal can be readily acquired by a simple photodetector and with well-known electronic techniques it can be locked to an external reference frequency. The error signal can be fed back to the oscillator to stabilize the usually significantly jittering pulse-to-pulse CE phase slip ($\Delta\phi$) which is due to mechanical and thermal instabilities and pump power fluctuations. This method is termed as self-referencing technique, f -to- $2f$, or v -to- $2v$ interferometry.

The physical channel of the error signal feedback can be different depending on oscillator architecture. The important point is that the relation between the group and phase velocities has to be changed. In a KLM oscillator where most of the dispersion is compensated by a prism pair in a double-pass setup a slight swivel movement of the end mirror (on which the spectrum is spatially dispersed) can be used to introduce a linear phase delay with frequency which is equivalent to changing the group delay (Reichert et al., 1999 and Jones et al., 2000). The disadvantage of this

method is higher CE phase noise that can be characterized by measuring the fluctuations in f_{ceo} delivered by the f -to- $2f$ interferometer. Since this method is based on mechanical feedback, bandwidth limitations also arise. Mirror-dispersion-controlled (MDC) KLM oscillators perform better from this point-of-view (Helbing et al., 2002), compared with their prism-dispersion controlled counterparts. Feedback is achieved by modulating the power of the pump beam with an electro-optic modulator thus affecting the oscillator dispersion through nonlinear coupling.

There are two major application fields of such oscillators corresponding more or less to the time-domain and the frequency-domain pictures of such a pulse train. The fact that the optical waveform evolves in a controlled manner if f_{ceo} is stabilized calls for investigations of the interaction of these waveforms with matter. This thesis deals with these issues. On the other hand, in the frequency domain the whole frequency comb is stabilized once f_{ceo} is locked to a stable reference frequency. This fact immediately calls for high precision spectroscopy applications, since the gap between the usual domain of rf frequency standards and optical frequencies can be bridged in a single step with a simple laser oscillator and some electronics (Cundiff and Ye, 2003). This was previously only possible with extremely complicated phase-coherent frequency chains (Schnatz et al., 1996) filling industrial-scale halls only affordable for a couple of huge federal standards institutes. This latter aspect of CE phase stabilization will not be treated further on in this thesis.

The above methods for CE phase shift measurements and stabilization rely on a pulse train in which the full repetition rate of the laser oscillator is preserved. In amplified laser systems, typically preserving only at most every thousandth pulse from the oscillator output a different approach is needed. The suggested and implemented idea for this is also based on SHG of the fundamental (single) pulse (Takehata et al., 2001), but instead of the beat signal between adjacent frequency comb lines the spectral interference between the spectrally overlapping parts of the fundamental and the second harmonic spectrum is measured by a spectrograph. The pulse-to-pulse CE phase shift is manifested in the fringe shift of the spectral interference pattern. Since current technology allows this to be obtained with kHz repetition rate, the full CE phase evolution of the output of an amplified, ultrashort-pulse laser system can be assessed, however, *only relative to an unknown CE phase offset.*

2.2 Overview of the building blocks of the laser system

The laser system I developed was based on an already existing KLM MDC oscillator with a long cavity (Poppe et al., 2001). The extra long resonator results in a lower repetition rate and a proportionally higher pulse energy holding promise of a better chance of inducing a CE phase sensitive effect expected to occur in highly nonlinear interactions.

The novel feature of the laser system (Fig. 4.) was that the output of the oscillator was split into two beams by a dielectric multilayer beam splitter. Only a fraction of the beam (15 %) was necessary for CE phase stabilization in a standard f -to- $2f$ interferometer, the rest could be used for some experiment, out-of-loop CE phase or pulse diagnostics. At that time this was a unique feature in terms of CE phase stabilized laser systems, since in most of these lasers at least half of the

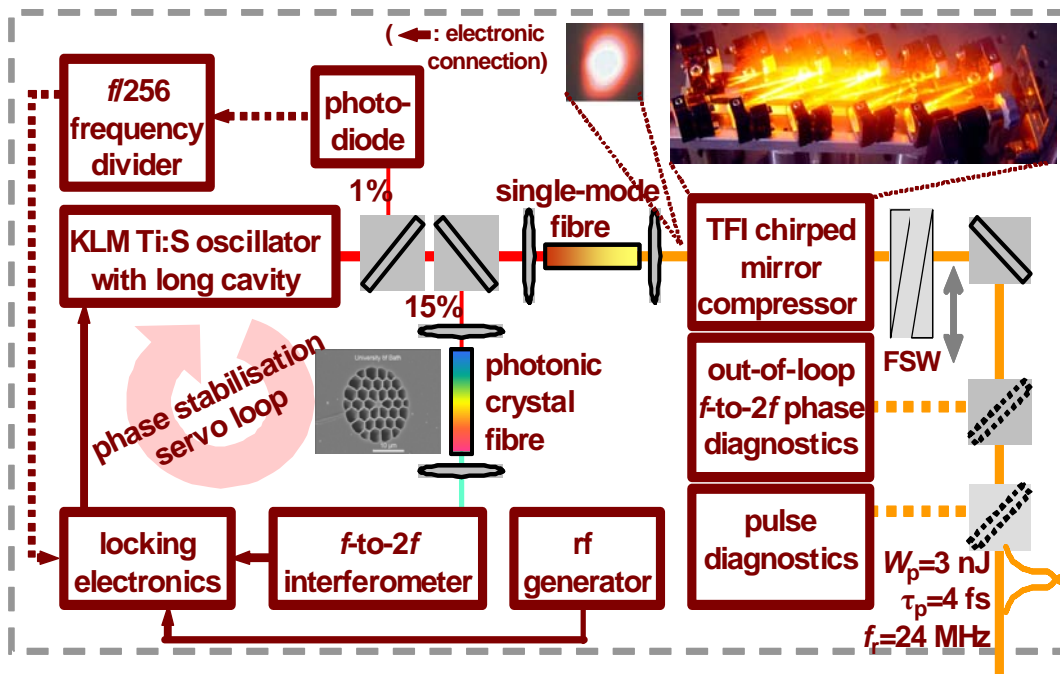


Figure 4. Overview of the building blocks of the laser system. Red and orange lines indicate the laser beam, dark purple lines are electronic connections (dotted lines are alternative beam paths or alternative electronic connections) FSW: fused silica wedge pair. W_p indicates the pulse energy. For a detailed description see text.

oscillator output was used for phase stabilization (e.g. Fortier et al., 2002a). Since in my case a long-cavity oscillator with 24 MHz pulse repetition rate was used with threefold output pulse energy (compared to standard, 70-80 MHz oscillators), measurements were made possible other groups did not have access to. Typically I had >20 nJ pulses at the oscillator output with 9-10 fs pulse length.

The split-off 15 % portion of the beam was broadened in a piece of PCF to reach octave spanning bandwidth. The type of fibre (the structure of which can be seen in Figure 4), focusing conditions, the polarization of the ingoing beam and pulse precompression (utilizing a separate pair of chirped mirrors) was carried out in such a way that the output spectrum from the fibre spanned an octave and separate spectral maxima could be reached at the wavelengths of 1000 nm and 500 nm making it ideal for f -to- $2f$ interferometry. The generated supercontinuum is depicted in Figure 5 also illustrating the efficiency of PCFs in generating white-light supercontinua with pulses having only nJ or sub-nJ energies.

During this setup procedure we also found by chance that using a 20- μ m-thin pellicle instead of a dielectric multilayer beam splitter surprisingly enhanced the extent of spectral broadening in the PCF at the same pulse energy (Fig. 5). This effect was later confirmed to be caused by stimulated Raman scattering interaction

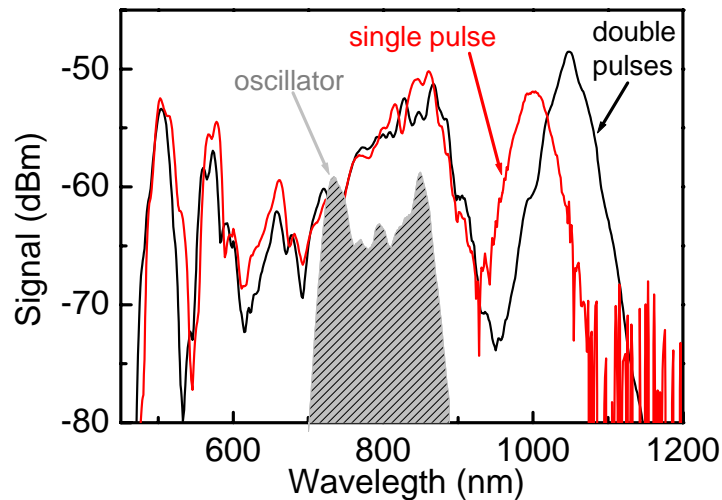


Figure 5. The generated supercontinua in a cobweb PCF of 6 mm length and 2.2 μ m core diameter with single (gray curve) and double (black curve) pulses of 0.8 nJ pulse energy and 11 fs duration. The spectrum of the input pulse is also shown (not to scale). Note the logarithmic y axis scale.

between the double pulses reflected from the front and the back surfaces of the pellicle separated by 150 fs in the PCF (Kalashnikov, Dombi et al., 2003). Using the optimized spectrum a standard Mach-Zehnder-type f -to- $2f$ interferometer was used (see Fig. 3, lower panel) and the error signal for the feedback was generated in standard phase-locking electronics and was applied to the electro-optic modulator changing the pump power in the oscillator.

The reference signal for phase locking was derived from two alternative sources. The first one was a Marconi rf signal generator set to $f_{\text{ref}} = 1$ MHz (solid electronic connections in Fig. 4). Since this frequency had no fixed relationship with the repetition rate of the laser whatsoever, one can only say that *roughly* every 24th pulse had the same optical waveform as a result of stabilization as it can be seen from equation (2). As an alternative, using a tiny portion of the beam the repetition rate of the laser could be picked with a photodiode and divided by 256 in a frequency divider resulting in a reference signal for the servo loop around $f_{\text{ref}} = 100$ kHz (solid-line electronic connection substituted with dotted-line ones in Fig. 4, where applicable). This way one could achieve an optical output in which *exactly* every 256th pulse had the same optical waveform. After testing both of them, I found, however, that this fundamental difference between the two alternative solutions does not really matter if one wants to carry out some phase-sensitive measurement with such a beam; it only makes a difference in terms of the performance of the servo loop, which was found to be better at $f_{\text{ref}} = 1$ MHz. The output of the laser system CE phase stabilized in such a way had to be further compressed to sub-5-fs duration to boost chances of inducing light-matter interaction that could show direct sensitivity to the CE phase.

2.3 Pulse compression with TFI chirped mirrors and pulse envelope diagnostics

The major portion (85 %) of the CE phase stabilized oscillator output consisted of pulses of 9-10 fs duration that was close to the transform limit allowed by the spectral width of the oscillator output. Further shortening the pulse therefore necessitated external spectral broadening in a fibre mainly on the basis of self-phase-

modulation (SPM) and other nonlinear effects, such as four-wave-mixing. The ideal medium for this was a short piece of single-mode telecom fibre with sufficiently small core diameter to enable tight focusing resulting in intensities high enough for sufficient SPM. Since the zero dispersion wavelength of such fibres lie in the mid-IR range I had to use as short a piece as possible, because the dispersion of the fibre itself had to be compensated with as few bounces off chirped mirrors (CMs) as possible. Experimentally found optimum parameters were $2.8\ \mu\text{m}$ for the core diameter (fibre manufacturer: 3M) and 1.5 mm for the fibre length. Smaller core diameters resulted in optical damage at the fibre entrance surface and longer fibre lengths did not provide a broader spectrum at the output indicating a nonlinear length being in this range. Even with these parameters one could observe stochastic damage effects after longer usage limiting the lifetime of the fibre to 2-5 days.

The shape of the broadened spectrum at the output of the fibre was also very sensitive to the actual cleave. Later on one will be able to see quite different spectral intensity distributions, for example in Figures 7 and 8. The centre of gravity of the spectra of the ultrashort pulses at the fibre output varied between 730 and 790 nm.

The pulse compression stage after the fibre output was realized by reflecting the pulses off 12 special CMs, called tilted-front-interface (TFI) chirped mirrors (Tempea et al., 2001). They contain the usual chirped multilayer structure but a novel solution was found to eliminate interference of beams reflected off the first layer and beams coming from inside the stack. In general, this interference poses a limitation to the bandwidth of CMs. Therefore, a thin wedge was contacted to the front surface of the mirrors changing the direction of the directly reflected beam thus avoiding harmful interference (Figure 6). Since this way there was some extra glass added to the mirror the amount of dispersion that could be compensated was smaller, therefore I had to use more of these mirrors. The extreme bandwidth (480 nm – 1030

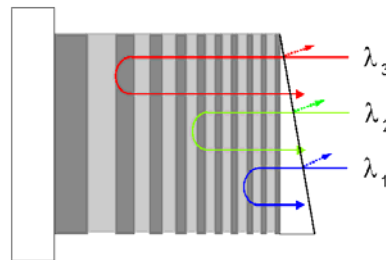


Figure 6. A tilted-front-interface chirped mirror structure. The beams with different colours illustrate its interference reducing effect, which increases its bandwidth.

nm) they supported both in terms of reflectance ($> 97\%$) and well-behaved group delay dispersion (GDD) was confirmed by pulse diagnostic measurements carried out with an autocorrelator adapted for extremely short pulses. At the output a thin wedge pair (FSW in Fig. 4) was also introduced so that the overall dispersion in the system could be fine-tuned by shifting one of the wedges.

Characterization of the spectral properties of the compressor can be carried out by measuring pulse spectra before and after the TFI mirrors. Fig. 7 shows the results together with the design reflectivity curve. One can see that the blue-shift suggested by higher reflectivity for lower wavelengths manifests itself in the measured spectra, too, since the centre of gravity of the spectrum is shifted from 811 nm to 790 nm. This, together with the blue-shift caused by nonlinearities during propagation in the fibre (self-phase modulation, four-wave mixing etc.) resulted in observed spectral centres of gravity as low as 710 nm after the compressor.

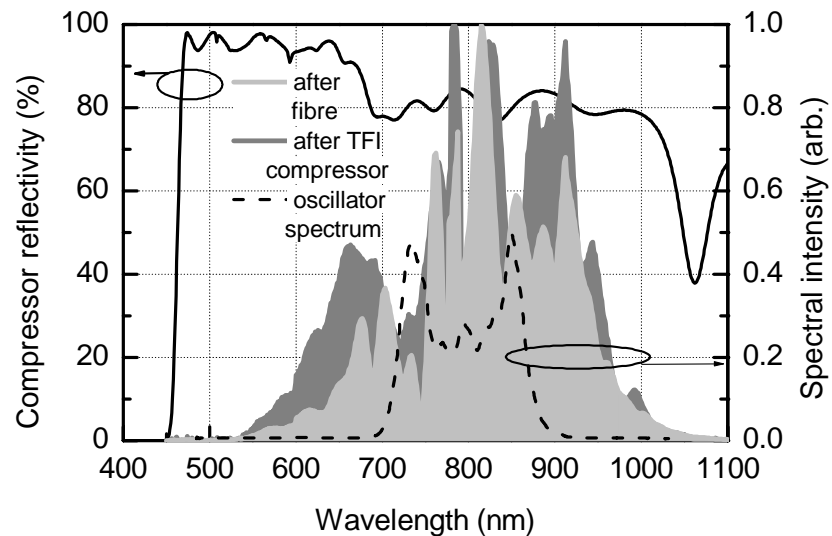


Figure 7. Spectral reflectivity curve of the TFI chirped mirror compressor and illustration of the blue-shift it causes with measured spectral intensity distributions. The center of gravity of the light gray spectrum is at 811 nm, whereas it is 790 nm for the dark gray one. The spectrum of the oscillator is also shown for reference.

Characterization of octave-spanning pulses is a challenging problem. Methods like FROG (Trebino et al., 1997) and SPIDER (Iaconis and Walmsley, 1999) are difficult to implement with weak sub-5-fs pulses since retrieving the spectral phase is plagued by the poor signal-to-noise-ratio, particularly in the spectral wings. We relied on a somewhat less involved and more robust technique: pulse reconstruction from the power spectrum and the second-order interferometric autocorrelation function (IACF) only (PICASO). It has been shown that the spectral phase is uniquely determined by the IACF and the power spectrum (Naganuma et al., 1989). Although there are debates about the accuracy of this approach (Chung and Weiner, 2001), successful pulse reconstruction has been demonstrated even in the presence of noise (Nicholson and Weiner, 2002).

I used a dispersion-free autocorrelator for recording the second-order IACF. The beamsplitter in the standard setup based on a Michelson interferometer was replaced by a thin (5- μm -thick) pellicle made of nitrocellulose. Brewster-angle-reflection-based polarization filtering was employed for separating the second harmonic from the fundamental field, since the spectra of the two signals overlap. The second harmonic is generated in a 9- μm BBO crystal phase-matched for 800 nm. Computer simulations showed that propagation effects (phase matching, group-velocity mismatch, and dispersive broadening) can be neglected in the evaluation of the pulse duration from the measured autocorrelation trace.

The power spectrum and the autocorrelation function of the compressed pulses are shown in Fig. 8. The algorithm used for pulse reconstruction is analogous to the PICASO algorithm (Nicholson et al., 1999 and Nicholson and Weiner, 2002), where the spectral phase is retrieved by means of minimizing of the difference between the measured IACF and that calculated from the measured power spectrum. This approach leaves some freedom in the mathematical representation of the spectral phase being optimized, since there are several ways of mapping a function of frequency onto a set of optimization parameters. In the original PICASO algorithm the phase is represented by a polynomial expansion and the coefficients of this expansion are optimized in order to retrieve the spectral phase.

This representation was compared with two other procedures. In one approach spline interpolation is used to construct the spectral phase as a smooth function from discrete values of the phase known at fixed frequencies; these values play the role of optimization parameters. In the second optimization scheme the optimized

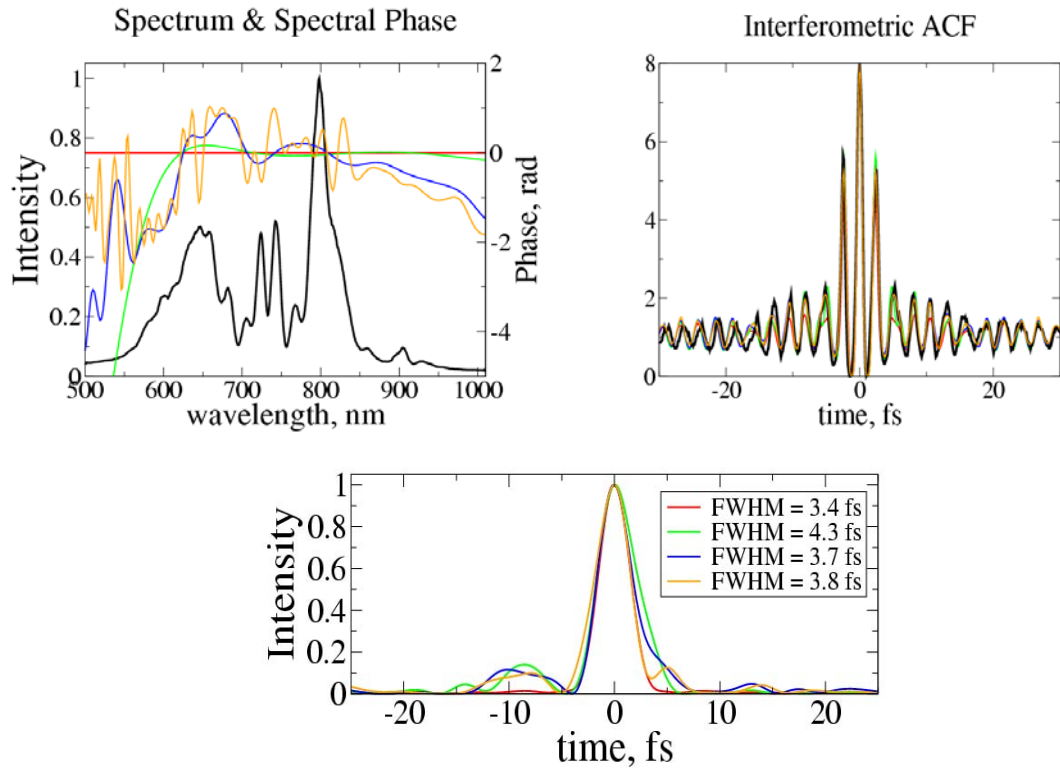


Figure 8. Details of pulse reconstruction from measured spectrum (black curve on first panel) and measured interferometric autocorrelation function (black curve on right panel). For best fitting the interferometric ACF different spectral phase functions were used, namely polynomial phase (green), spline phase (orange), spline GDD (blue) fitting and reconstructed data of a transform limited pulse are also given for reference.

parameters are the second-order derivatives of the phase. In both cases IACFs calculated from the retrieved pulses match the measured IACF better than the polynomial representation of the spectral phase (Fig. 8). This can be explained by the fact that the uncompensated GDD contains fast oscillations introduced by chirped mirrors, which the polynomial expansion of the spectral phase may not be able to track.

The FWHM of the retrieved pulses varies in these three cases from 3.7 to 4.3 fs, while the FWHM of the bandwidth-limited pulse with the measured spectrum would be equal to 3.4 fs. Figure 8. depicts the reconstruction that provides the best agreement between measured and computed IACFs. The pulse duration evaluated from this best fit was 3.8 fs, which was one of the shortest optical pulse lengths ever generated at the time of publication (Yakovlev, Dombi, et al., 2003).

2.4 Out-of-loop CE phase diagnostics

With the f -to- $2f$ phase-locking loop in operation, the CE phase slips by $\Delta\varphi = 2\pi(f_{\text{ref}}/f_i)$ from pulse to pulse in the main output beam of the laser system. It seemed useful to test the loop with a second, independent, out-of-loop f -to- $2f$ beat signal detector. To this end I focused the 4-fs pulses carried at $\lambda_0 \approx 710$ nm into a 0.1-mm-thick ZnO crystal. For optimized second harmonic generation of the infrared part of the broadband radiation the polished surface of the ZnO crystal has a crystallographic orientation of (1120). The second harmonic of the low-frequency spectral components near $\lambda_l = 1000$ nm beat with the high-frequency components around $\lambda_h = \lambda_l/2 = 500$ nm (as in Mücke et al., 2002), resulting in an f -to- $2f$ signal at 500 nm modulated at $f_{\text{ceo}} (=f_{\text{ref}}$ with the servo loop in operation). After spectrally filtering the beam passing through the crystal, this signal can be detected with a photodiode and with an electronic spectrum analyzer. The beat signal is typically 30 dB above noise in a resolution bandwidth of 10 kHz, which is of course not as good as in the phase locking Mach-Zehnder interferometer due to inadequate spatial mode matching and temporal walk-off of the fundamental and SH beams.

The beat component $S(t)$ of the signal of the out-of-loop f -to- $2f$ interferometer oscillates with a frequency f_{ceo} and can be written as $S(t) = S_0 \cos(2\pi f_{\text{ceo}} t + \theta)$. This signal is phase-locked to an external reference, $R(t) = R_0 \cos(2\pi f_{\text{ref}} t)$, yielding $f_{\text{ceo}} = f_{\text{ref}}$. As a consequence, phase-sensitive, narrow-band (lock-in) amplification is ideally suited to detect $S(t)$. The lock-in amplifier is able to measure directly both the amplitude S_0 and the phase θ or, alternatively, it can acquire the in-phase ($X = S_0 \cos\theta$) and the quadrature ($Y = S_0 \sin\theta$) components of the input signal (see Fig. 9). This latter pair of output parameters provides, of course, the same, full information on the signal to be measured as the S_0, θ parameter pair. Whilst this out-of-loop f -to- $2f$ measurement allows the jitter of φ to be determined, it is not suitable for measuring the CE phase itself due to an unknown phase offset φ_0 always inherently present in f -to- $2f$ phase detection. This aspect will be illuminated in more detail in Chapter 3.

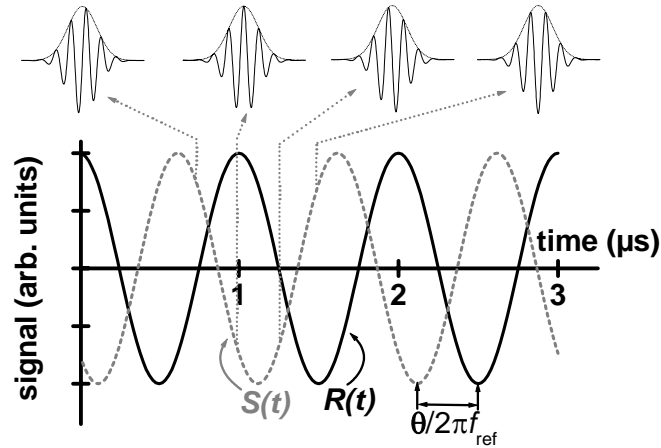


Figure 9. Principle of lock-in-detection with the evolution of the reference signal with $f_{\text{ref}} = 1$ MHz and the signal $S(t)$ to be measured. For some points of the reference signal the actual shape of the optical waveform for the corresponding pulse in the mode-locked pulse train is also depicted.

The resulting signal from the out-of-loop f -to- $2f$ interferometer at $f_{\text{ceo}} = f_{\text{ref}}$ can be characterized by measuring its intensity dependence. Since varying the intensity of an ultrashort pulse is not trivial without introducing additional wavefront distortions or pointing inaccuracies, it had to be realized by Fresnel reflecting a portion of the beam off 5- μm -thin pellicle beam splitters. Intensity variation was carried out by changing the angle of incidence of the beam on the beam splitter and using the transmitted portion. Because of the negligible thickness of the pellicle this did not distort the waveform too much and the lateral displacement of the beam was also negligible. This way I avoided any kind of additional dispersive, diffraction or pointing instability artefacts upon intensity variation that would render subsequent measurement data points incomparable.

Since, as stated above, the f -to- $2f$ beat signal was measurable with an electronic spectrum analyzer as well, I carried out the intensity dependence measurement with this device. Results can be seen in Fig. 10. The amplitude of the beat signal changes according to a power scaling rule with the input beam intensity with an exponent of 2, corresponding to the order of nonlinearity of the process used to generate the second harmonic beat component.

After this introductory measurement I tested the f -to- $2f$ beat in another way. The electronic spectrum analyzer does not yield any phase information regarding the signal to be measured. Therefore, to confirm that the observed signal indeed originates from the evolution of φ in the laser pulse train, I introduced a path of variable length through a pair of thin fused silica wedges (FSW in Figure 4) and measured the

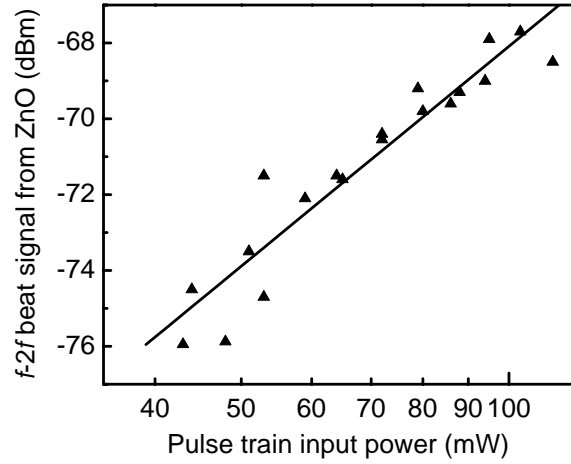


Figure 10. Intensity dependence of the f -to- $2f$ beat signal from the out-of-loop CE phase characterization setup and the linear fit showing a second-order power-law-scaling. Note the log-log scale.

variation of the in-phase component of the lock-in output, $X = S_0 \cos\theta$, as a function of the change ΔL in the fused silica path length. This way both the frequency and the relative phase of the in-loop f -to- $2f$ and out-of-loop f -to- $2f$ signals could be tested. Moreover, this serves as a test for the CE phase sensitivity measurement of any physical process that can be induced by the output beam of this laser. The result is shown in Figure 11. The sinusoidal oscillation in X is accounted for the fact that θ varies linearly with the path length, $\theta = \theta_0 + \pi(\Delta L/L_{f\text{-to-}2f})$, with the period length being evaluated as $L_{f\text{-to-}2f} = 20.9 \pm 0.7 \mu\text{m}$ from a least-squares fit (line in Figure 11) to the measured data (triangles), the details of which will be discussed below. This is in excellent agreement with the theoretical value of $L_{f\text{-to-}2f} = 21.5 \mu\text{m}$ (see later).

The rapid change of the oscillation amplitude indicates good pulse compression: since optimum dispersion balance of the whole compressor system can be realized only at a certain amount of the wedge material introduced in the beam, any kind of detuning from this state will result in chirped pulses, hence lower SH intensity in the out-of-loop f -to- $2f$ interferometer. In case of 4-fs pulses even some tens of microns of extra material in the beam can cause a chirp that reduces the SH signal noticeably.

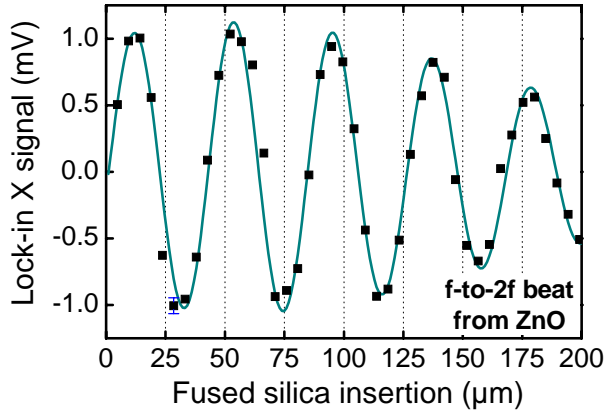


Figure 11. In-phase, $X = S_0 \cos\theta$ component of the lock-in amplifier output as a function of the change in path length through the fused silica glass wedges. The lock-in input signal is the f -to- $2f$ beat note from a ZnO crystal. The fit to the measurement data points was made on the assumption of an intensity dependence of the signal as $S_0 \sim I_p^x$ with $x = 2$. The peak intensity drops owing to dispersive pulse broadening upon propagation in the wedge material.

less phase jitter over similar acquisition times. However, in both of the referred studies two identical f -to- $2f$ interferometers were used: one in the stabilization loop and one for measurement. This gives rise to some cancellation of real noise of the CE phase because of common mode rejection via the similar amplitude-to-CE phase coupling mechanisms (Fortier et al., 2002b and Ames et al., 2003) in both interferometers. In our system the octave spanning light signal for the stabilization f -to- $2f$ interferometer is generated in a photonic crystal fibre completely different from the conventional telecom fibre in which the major portion of the beam is propagated. This results in higher sensitivity for the noise of the CE phase compared with the noise of the measurement system; therefore, the real CE phase noise at the output is overestimated and provides a reliable upper limit in my case.

Tracking the out-of-loop f -to- $2f$ signal in the time domain at a fixed value of ΔL over a period of 10 minutes yielded an rms carrier-envelope-phase jitter of less than 1.2 rad, indicating good long-term control of θ (and thereby ϕ) in the 4-fs pulse train. In similar laser systems more detailed out-of-loop studies of this effect were conducted (Fortier et al., 2002a, Witte et al., 2004), partly also by resolving phase noise spectrally.

These experiments yielded

3 Laser-solid interaction induced by controlled optical waveforms

In this chapter I will describe experiments that I conducted using the laser system described in Chapter 2. To my knowledge these are the first experiments ever in which the CE phase sensitivity of a laser-solid interaction process was investigated, therefore they can be regarded as the first “controlled optical waveform-solid interaction” studies. Apart from such an approach being interesting for basic research by itself, another goal of this work was to find a method that is capable of measuring the CE phase of a laser pulse on a single-shot basis, without the need for costly vacuum equipment, without relying on inefficient and not particularly easy-to-handle gas-phase interactions and using only low-energy pulses.

It was not obvious which class of interactions could candidate with best chances that could have such desired features. The output parameters of the laser determined the possibilities, of course, and since the pulse energy was limited to a couple of nanojoules a carefully designed experiment was required.

3.1 Overview of light-matter interaction from the CE phase sensitivity point-of-view

Light-matter interaction can be classified according to different sets of features that are relevant for one or another application. In terms of CE phase sensitivity the most crucial parameter is the intensity of the beam, not just because of potential nonlinear scalings, but mainly due to the interaction changing its nature with higher and higher intensities.

Well-known nonlinear processes occur in the so-called perturbative regime of nonlinear optics, where the laser field is much smaller than its atomic Coulomb counterpart and formally the polarization of an atomic ensemble can be expanded into a Taylor series with respect to the field. This also includes assuming

instantaneous response of the propagation medium to the electric field. Quantum mechanically the external field means only a perturbation of the atomic potential, hence the term perturbative nonlinear optics. Such typical processes include second harmonic generation (SHG), sum frequency generation, self phase modulation, stimulated Raman scattering, optical parametric processes etc., all known from standard nonlinear optics textbooks (Shen, 1984, Boyd, 1997). In this regime the evolution of the pulse envelope governs the interaction, which means that the CE phase does not come into play. For example, the CE phase changes the shape of the second order autocorrelation function of a laser pulse noticeably only in the sub-cycle pulse length regime, which is not accessible for (visible and near infrared) optical frequencies with current laser technology. The efficiency of these processes in the simplest cases show power scaling with the intensity, the exponent being determined by the order of the terms in the Taylor expansion having the major contribution. In this regime the main implication in terms of the CE phase is a fundamental property of a certain class of parametric interactions, where the CE phase value can automatically be stabilized in the output beam (Baltuška et al. 2002).

Harmonics can be generated not only in dielectrics but on metal surfaces, too. This well-known phenomenon could also provide a basis for CE phase measurement. According to a recent and experimentally not yet verified suggestion (Varró, 2004) one should generate surface harmonics with short enough pulses. The harmonic signal will then have peaks at $2\omega_L$, $3\omega_L$ etc. If the bandwidth of the generating pulses is sufficient these peaks become so wide that exactly half way between the harmonic maxima there will be a non-vanishing signal. Spectrally filtering this signal at $1.5\omega_L$, $2.5\omega_L$ etc. with a narrow-band filter and detecting this with a sensitive photomultiplier should provide a way of measuring the CE phase with somewhat higher pulse energies. This approach would be a more compact implementation of a previous, similar idea (Mehendale et al., 2000) based on harmonic generation in crystals. In both cases the CE phase effect pops up as a result of interference between different harmonic generation channels resulting in the same final photon energy.

When it comes to bound-free transitions a different wealth of phenomena can occur, such as multi-photon-induced electron emission or tunnel ionization. Both of them can be characterized in a broad parameter range and both for atomic media and solids within a single theoretical framework, called Keldysh theory (Keldysh, 1965)

that connects the two phenomena mentioned above. Without going into details the so-called Keldysh parameter has to be mentioned here given by the equation

$$\gamma = \omega_L(2mW_b)^{1/2} / (eE_0), \quad (5)$$

where m is the electron mass, e its charge, W_b is the binding energy of the most weakly bound electron (ionization potential or work function) and E_0 is the electric field amplitude. The theory yields well-known formulas for both boundary cases. For high frequencies and/or low field strengths and/or high ionization potentials, where $\gamma \gg 1$ one gets a non-adiabatic electron emission with the well known scaling rule of $j \sim I^n$, where j is the emitted photocurrent, n is given by $n = [W_b/\hbar\omega_L + 1]$ (square brackets indicating the smallest integer less than the argument) and the intensity I has the fixed relation with the field amplitude by $I[\text{W/cm}^2] = (1/2Z_0)E_0^2[\text{V/m}]$ (Z_0 is the vacuum impedance, $Z_0 = 377 \text{ V/A}$). For the other extreme, $\gamma \ll 1$, one gets the well known formulas for tunneling emission, which is adiabatic, following the field evolution instantaneously. For the region in between, where $\gamma \sim 1$, conclusions of the theory are not that simple, but analytic, closed-form results are still available (Yudin and Ivanov, 2001).

Light-matter interactions involving bound-free transitions can be thus classified according to the value of γ (limiting ourselves to the two extremes) and the medium (solid or gaseous). For CE phase sensitive applications two of the four possibilities became important.

When low-energy, long-wavelength laser beams interact with metal surfaces electrons are freed via multi-photon induced surface photoelectron emission (MSPE)*. This process is a fundamentally perturbative and intensity dependent one and as such it was expected to be governed by the pulse envelope as in the case of nonlinear interactions taking place in dielectric media. It was recently found, however (Lemell et al., 2003), that this parameter regime and this interaction type can also provide high-contrast, CE phase sensitive phenomena. The next Section

* It has to be mentioned that observations similar to MSPE took place well before the advent of lasers and the Keldysh theory. In 1886-1888 Hertz and Hallwachs observed the emission of electrons from a metal surface when light of sufficiently high frequency impinges on it. The so-called "light electricity" was explained by Einstein in 1905, for which he received the Nobel prize in 1921. The photon approach of Einstein allowed early experiments to be explained: the photoelectric effect takes place when the photon energy exceeds the threshold for freeing the electrons from the metal. If it occurs, the number of electrons emitted depends on the light power (i.e. the number of incident photons) and its polarization. In addition to these parameters, improvement of laser technology allowed scientists to pose the question, whether this process depends on the actual optical waveform, too.

describes possible reasons for this in detail. I also conducted extensive experiments with this phenomenon which is the main topic of Chapter 3.

In gaseous, atomic media tunnelling emission sets an electron free, the motion of which is governed by the laser field. Provided that the field is linearly polarized the electron returns and hits the ion. The recollision process can take place elastically (the corresponding phenomenon is called above threshold ionization, ATI, Agostini et al., 1979), inelastically, through the ionization of a second electron (non-sequential double ionization, NSDI) or recombination can occur with the emission of an XUV photon (HHG). Since these processes are governed by the laser field directly, CE phase sensitivity is expected provided that one has short enough pulses.

The first signature of CE phase effects was observed for ATI manifesting in spatial and (electron) spectral CE phase sensitivity of the electron emission process (Paulus et al., 2001, 2003). However, the sophisticated detectors needed (for high contrast) and the low-efficiency gas-phase nature of the interaction (which usually manifests in the requirement of at least μJ -energy pulses) does not make this the most attractive method for single-shot diagnostic CE phase detection. Typically an on-target intensity of around 10^{13} W/cm^2 is required, which involves the focussing of a significant portion of the output of an amplified laser system into the gas jet. The CE phase sensitivity of HHG was scrutinized in the Motivation section of this thesis because of its serious implications in attosecond science. A very recent experiment proved that NSDI is also governed directly by the laser field (Liu et al., 2004).

Besides these approaches requiring moderate pulse energies readily available from amplified Ti:S laser systems with kHz repetition rate, another experimentally not yet explored field of the application of sub-10-fs laser pulses (and therefore of potential interest from the CE phase point-of-view, too) could be in a higher intensity range, where the electron could even attain relativistic velocities during its field-induced motion. One exciting application is the generation of monoenergetic electron beams by laser wake field acceleration. This holds the potential of large-scale particle physics facilities being substituted with table-top laser systems. The state-of-the-art in the generation of such beams provides electrons with MeV energies, however, recent breakthrough experiments (Mangles et al., 2004, Geddes et al., 2004 and Faure et al., 2004) were carried out using relatively long, 30-40 fs laser pulses. Provided that a laser system is constructed delivering 5-fs laser pulses carrying 5 mJ

pulse energy with the desired high prepulse contrast brand new effects could be observed in laser-driven electron acceleration (Pukhov and Meyer-ter-Vehn, 2002).

3.2 Theoretical basis of CE phase sensitivity of multi-photon photoemission

Recent simulations of the MSPE process based on time-dependent density functional theory carried out by Lemell et al. in 2003 predicted that the photoelectron yield of emission from a metal surface (modelled as a confined free-electron gas using the jellium model) exhibits a robust dependence on φ in a parameter range broad enough for practical use. Several conditions have to be met, though. The first and most intuitively justifiable one is that the pulse must be short enough to contain just a few oscillation cycles. Pulses significantly shorter than 10 fs are required at $\lambda_L = 750$ nm, where $T_0 = 2.5$ fs, to induce a substantial variation of the photocurrent with φ , as shown in Figure 12.

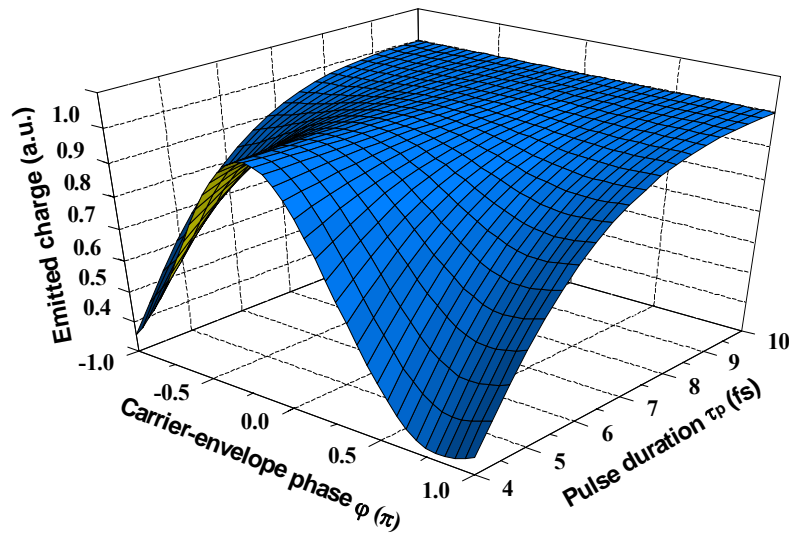


Figure 12. Computed charge emitted from a gold surface (modelled as a confined free-electron gas (jellium); for further details see Lemell et al., 2003) exposed to a Gaussian laser pulse ($\lambda_0 = 750$ nm, $I_p = 5 \times 10^{12}$ W/cm²) at grazing incidence as a function of the CE phase φ . Pulse durations are ranging from 4 fs to 10 fs. The light is incident with the electric field oriented along the surface normal ('P' polarization). The carrier-envelope phase is defined by $E(t) = A(t)\cos(\omega_L t + \varphi)$ with $E(t) > 0$ implying a field directed into the irradiated matter.

In the simulation geometry the laser pulse impinged on the surface at grazing incidence and ‘P’ polarization with an on-axis peak electric field of $E_{\perp} \approx 6 \times 10^7$ V/cm, corresponding to a peak intensity of 5×10^{12} W/cm². The material chosen was gold with a work function (W) of approximately 5 eV, implying that simultaneous absorption of at least three photons (with a typical laser wavelength of 750 nm) is needed for emission to take place. These parameters yield $\gamma \approx 3$ according to equation (5). The intensity required for $\gamma = 1$ would be roughly 5×10^{13} W/cm².

It can be seen in Fig. 12 that for a 10-fs, 750-nm pulse there is hardly any observable difference between the electron yield of a *cosine* pulse ($\varphi=0$) and a *minus cosine* pulse ($\varphi=\pi$), whereas at $\tau_p = 4$ fs, a drastic phase effect is seen. Similar conclusions were recently drawn from phenomenological considerations (Helbing et al., 2003). Simulations have also revealed that the emitted charge per pulse has a maximum at a phase value of $\varphi_{\max} = -\pi/4$ (see Fig. 12), implying maximum strength of the electric field (pulling the electrons away from the surface) some 300 attoseconds after the pulse peak, and that it is invariant to the temporal structure and peak intensity of the pulse shape in the regime of multi-photon ionization.

In numerical studies following the publication of Lemell et al., 2003, the phase sensitivity was checked for the most commonly used analytic intensity profiles (i.e., gaussian, sech^2 and \cos^2), for some specific analytic pulses with pre- and postpulse satellites and for some typical reconstructed intensity profiles delivered by our laser system (Yakovlev, Dombi, et al., 2003 and see Section 2.3). In all of these cases the same quantitative behaviour was found with merely the modulation depth (i.e. the extent of the sensitivity of the total emitted charge to the CE phase) being subject to slight pulse shape dependence. From these extensive analyses $\varphi_{\max} = -\pi/4 \pm \pi/10$ CE phase calibration value can be derived, showing the CE phase value at which maximum electron yield is expected. The uncertainty originates from limitations of numerical accuracy.

The major drawback of this theoretical approach is the limited physical insight it allows into the nature and dynamics of the photoelectron emission process. Physical mechanisms and emission channels are veiled by numerics. The simulation procedure is computationally also very involved with days of PC processor time needed for relatively small simulation grids. It was these drawbacks that prompted an

alternative approach to find a mechanism behind potential CE phase sensitivity of MSPE and surprisingly a very simple and illustrative model can support major conclusions drawn from the previous one.

This alternative approach to be presented here in detail is inspired to a certain extent by the simple and easy-to-visualize approach of P. B. Corkum's three-step semiclassical model of high harmonic generation (Corkum, 1993) the consequences of which are in remarkable agreement with the results of a rigorous quantum mechanical treatment of the process (Lewenstein et al., 1994). In that case of gas-phase atomic ionization induced by the field of a laser pulse the electron is assumed to be „born” in the continuum with zero initial velocity after tunnelling through the potential barrier distorted by the laser field. After that it is treated as a free particle and its movement is examined in the potential of the laser field only. Provided that the beam is linearly polarized the electron wave packet returns to its parent ion after a certain wiggly motion in the laser field and recombines with the ion with some finite probability. The result is the emission of high-harmonic photons the energy of which is determined by the ponderomotive potential and the binding energy. Obviously, the time of birth, the instant of this recombination, and consequently the temporal and spectral characteristics of the XUV emission are also influenced by the carrier-envelope phase of the laser pulse if the generating pulses have few-cycle duration.

A somewhat analogous picture can be constructed for multi-photon induced photoelectron emission from solid surfaces (MSPE). The first step corresponds to instantaneous electron emission as a result of which a free electron is “born” somewhere near the surface. Since the light intensity is in the range typical of the perturbative regime of multi-photon absorption, electrons are emitted with low kinetic energy ($< \hbar\omega_L$) within a narrow time interval tightly centred at the peak of the pulse envelope. It can be assumed that the probability of the emission is proportional to $A(t)^{2n}$, with n being the order of the process, according to the perturbative nature of MSPE and well-known, justified intensity dependence laws that were found to be valid down to the few-cycle regime (Dombi et al., 2005).

After that, in a first approximation these electrons are steered in vacuum by the laser field, which is much stronger than the static electric field applied to extract and observe the photoelectrons and it is also stronger than the mirror-charge field. I justified the neglect of this latter potential by numerical proofs.

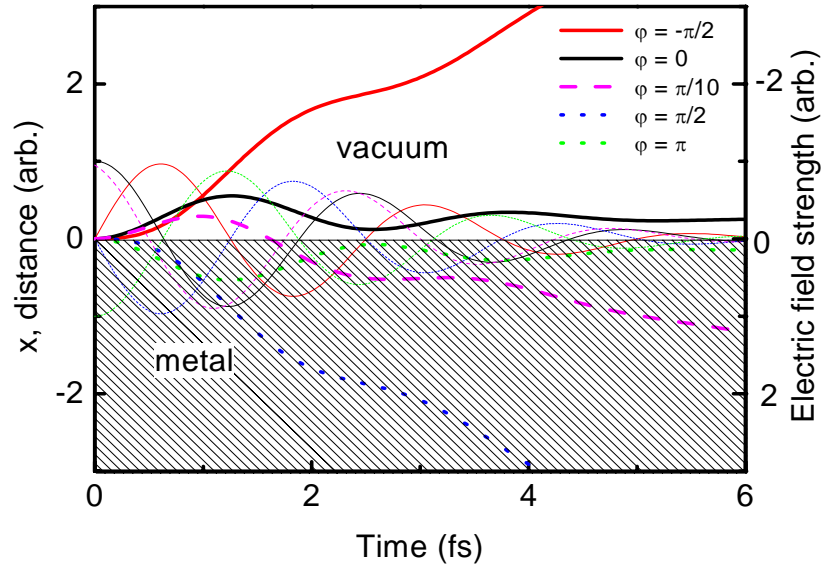


Figure 13. Classically computed trajectories (thick lines) of the emitted photoelectrons in vacuum above the surface of the cathode (positioned at $x = 0$) upon interaction with the field of the laser pulse (thin lines, note the reverse axis) for different CE phases. The electron is assumed to be emitted at the peak of the laser pulse envelope ($t = 0$). Outside the favoured range of $-\pi/2 \leq \varphi < 0$ (black and red curves) the electrons will be pushed back onto the surface by the electric field of the laser pulse either right after their bound-free transition (green and blue curves) or after performing a wiggle in the laser field (magenta curve).

On the basis of this picture I determined several electron trajectories by solving the classical equations of motion numerically and I found that for carrier-envelope phases in the range of $-\pi/2 \leq \varphi < 0$ the electrons undergoing bound-free transition at the peak of the pulse envelope are initially pulled away from the surface and never return during the pulse (see thick solid red and black curves in Figure 13). If the CE phase value is outside this distinguished “escape range” there are two different possibilities. The first is that at the time of birth of the electrons (at the pulse peak) the instant field points away from the surface and immediately pushes back the electrons into the metal (thick dotted blue and green curves, Figure 13). Recapturing of the electrons by the metal can also happen somewhat later, after they perform a wiggle in the laser field (thick dashed magenta curve in Figure 13).

It is a unique feature of few-cycle laser pulses that multi-photon-induced bound-free transitions are distributed over a period shorter than the optical cycle at the peak of the pulse envelope. This is expected to result in the sensitivity of the centre-of-

gravity motion of the electron cloud to the CE phase and in maximum electron extraction efficiency near the centre of the above determined “escape range”, i.e. at around $\varphi_{\max} = -\pi/4$. From these arguments it is also obvious that for longer pulses the broad temporal distribution of bound-free transitions along the pulse blurs the phase sensitivity of MSPE.

I quantified this argumentation by considering that the electron is not necessarily emitted at the pulse peak, but anywhere else during the pulse with a probability proportional to $A(t)^{2n}$. In each case one can determine the favourable CE phase interval in which the electron is allowed to escape from the surface. Overlapping these intervals with their corresponding weights ($A(t)^{2n}$) results in a histogram-like distribution (Fig. 14) which is equivalent to the electron yield as a function of CE phase already computed with a radically different method (Fig. 12). The qualitative agreement of these two is the more remarkable knowing that they were generated by two completely different methodology. The maxima of electron emission peaks with respect to the CE phase are roughly at the same positions ($-\pi/3$ for the curves in Fig. 14, subject to slight pulse length dependence) and the modulation depth of the emitted current is also correct to within $\pm 10\%$. Deviations from in terms of the shape

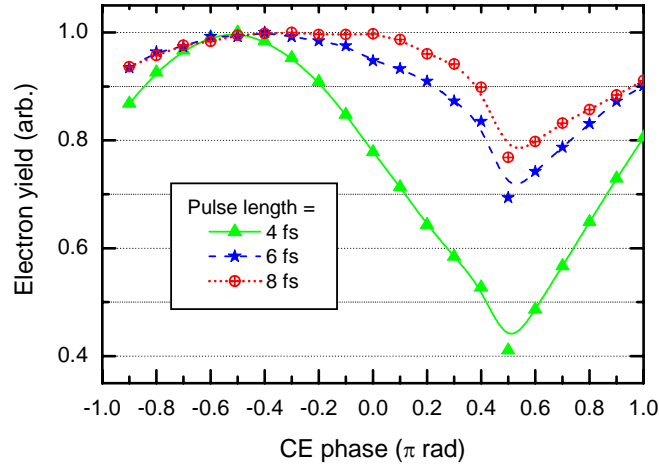


Figure 14. Computed charge emitted from a gold surface (modelled according to the phenomenological model described in Section 2) exposed to a Gaussian laser pulse ($\lambda_0 = 750$ nm) with intensity in the perturbative limit plotted as a function of the CE phase φ . The parameter for the set of curves is the pulse duration, ranging from 4 fs to 8 fs. The light is incident with the electric field oriented along the surface normal (‘P’ polarization, grazing incidence).

of the CE phase dependence curve can only be observed for longer pulses and could be attributed to some artefact in the computation procedure given the irregular curve shapes towards longer pulse lengths and the unrealistically preserved, relatively high modulation depth.

Another important requirement for a pronounced and robust phase effect is the dominance of multi-photon-processes in photoelectron production (Lemell et al., 2003). Even though some sensitivity to the CE phase prevails at higher intensities, in the tunnelling regime the phase calibration will be different, i.e. the position of the maximum of the signal, φ_{\max} in Figure 12 will be located at a different carrier-envelope phase value (Lemell et al., 2003).

The reduction of phase sensitivity at higher intensities seems somewhat surprising at first glance since, taking into account the adiabatic nature of tunnelling emission as opposed to the multi-photon regime (which is clearly seen in Figure 2. of Lemell et al., 2003), one would expect a less pronounced phase effect in the latter. The simple picture described above, however, can explain the strong phase effect expected in the multi-photon case as well.

3.3 Multi-photon photoemission experiments with controlled optical waveforms

Having the laser system described in Chapter 2 with the pulse diagnostics and tested by the out-of-loop, f -to- $2f$ CE phase diagnostic system, the measurement apparatus can be used for studying the CE phase dependence of multi-photon-induced photoemission from a metal surface. For the generation and low-noise pre-amplification of the photocurrent I used a commercial electron multiplier tube (EMT) equipped with a gold photocathode (R595, Hamamatsu), kept under 10^{-5} mbar. The laser beam was focused onto the cathode with an off-axis parabola with an f-number of 2 at an angle as close to grazing incidence as allowed by the vacuum chamber geometry ($\approx 70^\circ$). The adapted version of the setup depicted on Figure 4 can be seen in Figure 15, with only those components shown that are relevant for this CE phase measurement experiment.

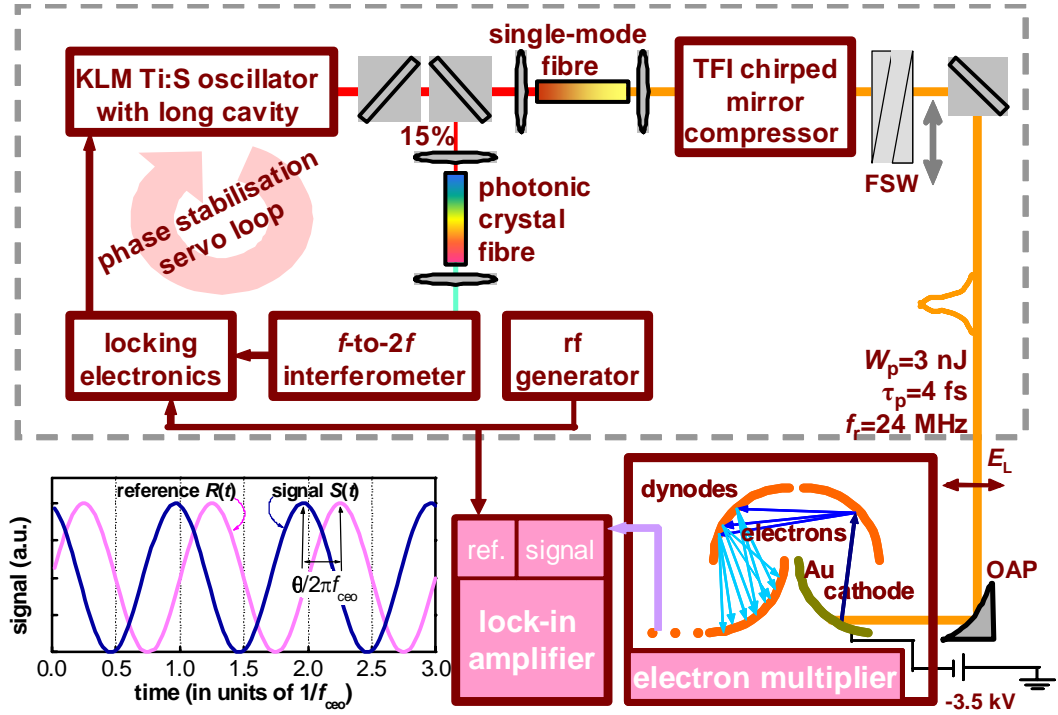


Figure 15. The relevant components of the CE phase stabilized laser system and the experimental setup used for measuring the CE phase with the help of MSPE. FSW: fused silica wedge, OAP: off-axis parabola.

With a spot diameter of $7 \mu\text{m}$ the on-target peak intensity was $I_p \approx 2 \times 10^{12} \text{ W/cm}^2$, corresponding to a peak electric field strength normal to the surface of $E_{\perp} \approx 4 \times 10^7 \text{ V/cm}$. In the $10^{12} - 10^{13} \text{ W/cm}^2$ peak intensity range the time-averaged output current from the electron multiplier tube (having a typical gain of 4×10^7), measured with an electronic spectrum analyzer, was found to follow a power-law scaling, $\propto I_p^n$ (Figure 16), indicating multi-photon-induced transitions. The evaluated value of n between 3.2 and 3.7 can be reconciled with the approximately 5-eV work function of gold and the spectral intensity distribution of the laser pulses. From the measured value of the output current I could also conclude that the number of the emitted electrons from the cathode was less than one per laser shot.

As a further preliminary test I measured the dependence of the non-linear photoemission signal on shifting of one of the fused silica wedges by ΔL at the output of the pulse compressor (FSW in Figure 15). The amplitude of the output signal from the multiplier tube, S_0 , measured with the lock-in amplifier referenced to the repetition rate of the laser, f_r , exhibits a rapid decay with ΔL as a consequence of

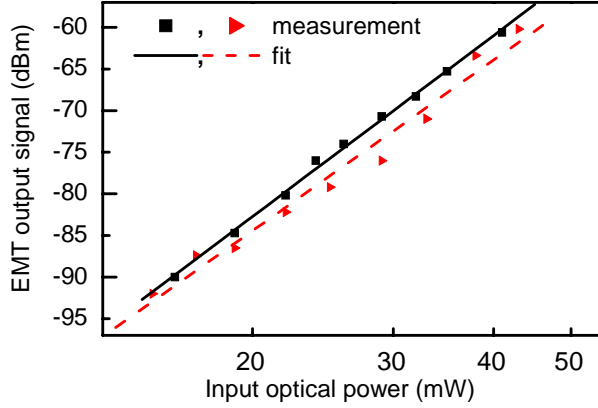


Figure 16. Intensity dependence of the output signal of the electron multiplier tube (EMT). x axis: average power delivered by the pulse train measured before the TFI chirped mirror compressor, logarithmic scale; y axis: output signal of the EMT (logarithmic scale, too) at the pulse repetition rate measured by an electronic spectrum analyzer. The power-law scaling of the photoemission signal is characteristic for the multiphoton regime. The linear fit to the measured data points resulted in slopes of 3.6 ± 0.1 and 3.4 ± 0.2 , respectively.

(envelope) shape from our pulse diagnostic system (Section 2.3) and simulating its linear, dispersive propagation in the wedge material (fused silica). The computed value of the peak intensity at each wedge position can then be raised to the power of n to fit the curve. Optimization yielded $n = 3$, resulting in the dashed envelope fit in Figure 17. Indeed, the photoemission is expected to be a third-order process for most of the photons of the laser pulse, and this method also corroborates previous pulse diagnostic results (Section 2.3) since a very unrealistic pulse shape would make the best-fit n value differ much more from the independently measured one (see Figure 16).

After these diagnostic and preparatory measurements I focused on checking the phase sensitivity of photoelectron emission. As φ evolves with a constant rate in the phase-controlled pulse train, it will create a modulation at the frequency f_{ref} in any φ -sensitive physical measurable, $S(t) = S_0 \cos(2\pi f_{\text{ceo}} t + \theta)$. Because the f -to- $2f$ interferometer is used to phase-lock the evolution of φ , the photoelectron emission will itself be phase-locked to the reference signal, $R(t) = R_0 \cos(2\pi f_{\text{ref}} t)$. However, as

dispersive effects. Although the pulses broaden only by a few percent upon travelling a distance of a few tens of micrometers in fused silica, the resultant decrease in their peak intensity is sufficient to lower the photocurrent appreciably, owing to the higher-order I_p^n scaling discussed above (Figure 17, triangles). An excellent fit to these measurement points can be achieved by taking the retrieved temporal pulse

discussed above, there will be a constant, non-vanishing phase offset θ between the $R(t)$ and $S(t)$.

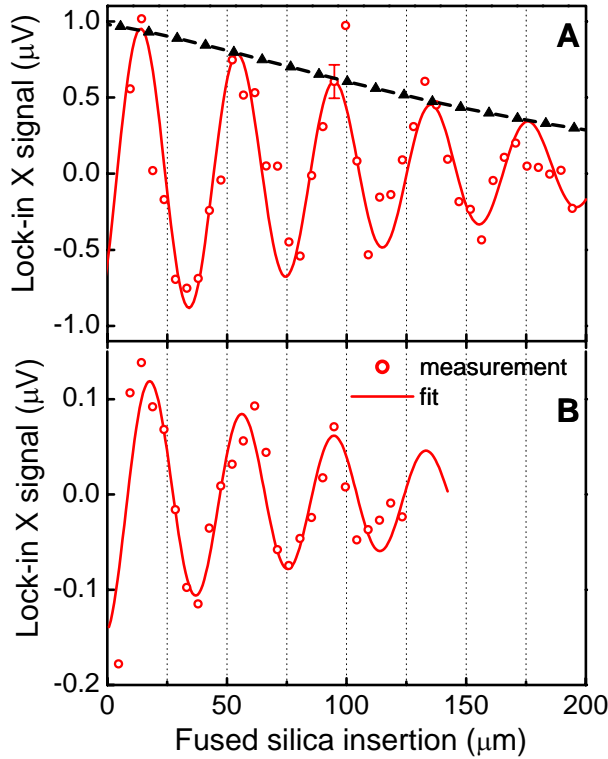


Figure 17. In-phase, $X = S_0 \cos\theta$ component of the lock-in amplifier output as a function of the change in path length through the fused silica glass wedges. The lock-in input is the photoemission signal amplified by the electron multiplier tube. The experimental data (circles) are corrected for a constant (non-oscillating) phase offset of electronic origin. Measuring the glass insertion dependence of the output signal of the electron multiplier tube with the lock-in amplifier referenced to the repetition rate of the laser and the subsequent fit yield the black triangles and the black solid fit. The latter is then used as an envelope function to fit the oscillating lines, giving excellent reproduction of the observed decay in the photoemission signal. The error bar depicts the rms fluctuation of the signal at a fixed ΔL over an acquisition time of 10 minutes, which is approximately equal to the time taken to collect the data. The two panels depict measurements with slightly different pulse lengths (4.5 fs for panel A, 3.7 fs for panel B).

Using a lock-in detector both the amplitude S_0 and the phase θ of the input signal can be determined. The important feature of the photoelectron emission signal is that the function $\varphi(\theta)$ can be given with sufficient accuracy, unlike in the case of the f -to- $2f$ signal coming from the ZnO crystal. For this the simple relation $\varphi(\theta) = \theta + \varphi_{\max} + 2\pi f_{\text{ref}} t$ is used, where φ_{\max} is the carrier-envelope phase that maximizes the physical measurable $S(t)$. The knowledge of φ_{\max} follows from simulations (see Section 3.2). This procedure then implies full information on how the evolution of φ in the pulse train is phased to the reference signal (i.e. at which phase of the reference signal a pulse with, for example, $\varphi = 0$ is interacting with the surface) and thus knowledge of the carrier-

envelope phase in any of the emitted laser pulses.

With the servo loop in operation and the lock-in amplifier referenced to f_{ref} , I observed a clearly measurable AC component $S(t)$ of the photoemission signal induced by the phase-controlled 4-fs pulses. Varying the insertion of the fused silica wedges gave rise to oscillation of the in-phase (X) component of the output of the lock-in amplifier with a periodicity similar to that observed for the f -to- $2f$ signal (circles in Figure 17), indicating that the observed signal originates from a continuous CE phase slippage in the pulse train. The effect was observed only when the sample was moved slightly out of focus, this being attributed to the fact that due to the large angle of incidence applied here different parts of the beam in the focal vicinity were incident with significantly different Gouy phase shifts exerted on them, which, in general, significantly modifies the phase of any electromagnetic or mechanical wave near the focus (Siegman, 1986 and Lindner et al., 2004). Thus, detrimental effects are expected to occur due to inherent spatial averaging unless one moves the surface as far off focus as allowed by the signal level. This observation also serves as subsidiary proof that the device was indeed delivering the first experimental verification for the CE phase sensitivity of MSPE.

Besides the clear oscillation of the $X = S_0 \cos\theta$ component of the lock-in output, its amplitude S_0 also exhibits rapid decay with ΔL as a consequence of dispersive effects, as discussed above. Since I could use the independently determined curve depicted on the same graph as the envelope function, the only fit parameter used for matching the experimental data appears in modelling the shift of θ with ΔL , $\theta = \theta_0 + \pi(\Delta L / L_{\text{MSPE}})$. The characteristic propagation length causing a π phase shift in the modulation of the photoemission signal was evaluated as $L_{\text{MSPE}} = 20.3 (+2/-1.5) \mu\text{m}$ from the fit in Figure 17, panel A. For panel B $L_{\text{MSPE}} = 19.3 (+2.7/-1.9) \mu\text{m}$ was found. These values are in good agreement with the computed dephasing length for the 4-fs, 710-nm pulses in fused silica, $L_{\text{deph}} = 22.5 \mu\text{m}$, specifying the propagation length over which the carrier-envelope phase suffers a π phase shift, converting $E(t)$ into $-E(t)$, assuming an unchanged pulse envelope. Structures in an ultrabroadband spectrum may cause the dephasing length to deviate appreciably from the approximative formula given in Brabec and Krausz, 2000. This applies in my case where the structured pulse spectrum results in $L_{\text{deph}} = 21.4 \mu\text{m}$, which is some 5% smaller than predicted by the analytic formula

given above for fused silica at $\lambda_0 = 710$ nm. This phenomenon will be examined in detail in Chapter 4.

Although the phase dependence of the photocurrent was clearly observable in my experiments, the depth of modulation caused by the slippage of ϕ is well below one percent, i.e. significantly smaller than predicted, for example, by Figure 12 for similar conditions. The origin of this contrast reduction will be more thoroughly investigated in the next section, but some potential reasons may be identified here, too.

Surface roughness of the pressed metal cathode coated with gold (as confirmed by atomic force microscopy scans) may reduce the fractional area exposed to a strong E_{\perp} and thereby the phase-sensitivity of the overall current emitted. This is because there is not expected to be any CE phase dependence caused by the field vector component that is parallel to the surface (as follows from, for example, the simple picture in Section 3.2). These irregularities can compromise phase measurement in one more way, since local field enhancement on them can result in tunnelling photoelectron emission. The CE-phase-dependent modulation of multi-photon-induced emission is phase-shifted by π as compared to the tunnelling regime (Lemell et al., 2003). This can obviously result in drastic contrast reduction when the surface-integrated emission signal is measured. Surface contamination owing to poor vacuum conditions (10^{-5} mbar) and sample preparation can also reduce CE phase sensitivity. Experiments on ion-induced electron emission (Winter, 2002) (where the Coulomb field strength exerted by the incoming projectile is comparable to the laser field in my experiments) confirmed that agreement between experiment and theory can only be achieved with atomically clean surfaces under ultrahigh vacuum conditions. Thus experiments on crystalline samples kept under higher vacuum are needed to test these hypotheses.

Additionally to these sample-based sources of contrast reduction, deterioration of the CE phase sensitivity can be rooted in imperfect phase stabilization. It is well known from the literature, but also suggested by common sense that, for example, mechanical noise of the f -to- $2f$ interferometers, amplitude-to-phase coupling in the fibres used for external spectral broadening (Fortier et al., 2002b and Ames et al., 2003) etc. are all noise sources that – if they appear within the phase-locking servo loop – will be written back onto the output of the laser and will appear as an extra

phase noise source in an out-of-loop measurement. This effect, already scrutinized at the end of the previous section, obviously smears the CE phase contrast of the photoemission signal, too.

A rough estimation from the measured rms phase noise value (see Section 2.4) yields a contrast reduction of at most 50% in my case, as it can be seen from Figure

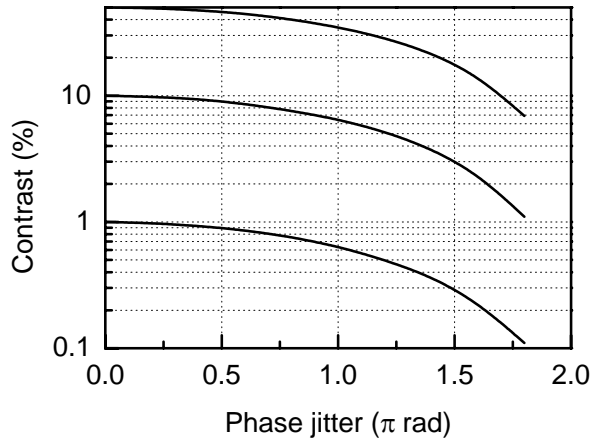


Figure 18. Reduction of CE phase contrast of any CE phase sensitive physical effect due to CE phase noise. Phase jitter was defined by assuming a top hat distribution of the CE phase of pulses within the range given by the x axis. The parameter of the curves is the initial contrast of phase sensitivity given by the y -axis intersection of the curves

18. The contrast is defined as the difference between the maximum and minimum values of the signal divided by the sum of them. The curves assuming a top hat distribution of CE phases within the given (e.g in this case ± 1.2 rad) CE phase noise range, which comes from the upper estimate for CE phase noise already mentioned at the end of Section 2.4. Since phase noise is obviously does not have a top hat distribution,

this rough calculation delivers an overestimation again which together with the overestimated nature of the original 1.2 rad phase noise itself means that the established 50 % contrast reduction value is definitely an upper estimation for the maximum possible phase noise in the system and thus can not explain contrast reduction by itself.

Improving beam pointing stability in the laser system as well as vibration and air flow isolation should thus improve contrast, too, by reducing the detrimental effects of this source of phase noise. Nevertheless, phase noise alone can not explain the discrepancy observed between theory and experiment.

3.4 Diagnostic and time-resolved measurements of multi-photon photoemission with few-cycle pulses

In spite of the technical reasons mentioned at the end of the previous section the fact that the photoelectron emission process showed much lower sensitivity with respect to the CE phase prompted further, more thorough investigations. These basic measurements can reflect how the general QED photon-electron interaction laws manifest at special new conditions (for example, for few-cycle pulses), with the eventual occurrence of new processes here. On the other hand, once known, the knowledge of these fundamental QED characteristics could be applied in different other research fields such as, for example ultrafast photoelectron sources and detection. Therefore, direct experimental check of several of these fundamental processes seemed to be useful.

The experimentally measurable basic features are reflected by the relation $j \propto |E_{\perp}|^{2n}$. The dependence of the photocurrent j on the E_{\perp} component variation presents the polarization dependence, which may prove the surface (vectorial) character of the photoemission process. The dependence on the intensity $|E_{\perp}|^{2n} \propto I_p^n$ (where I denotes the peak intensity of the laser pulse), demonstrates the n -th order perturbative multi-photon character of the interaction, as already demonstrated in preceding sections. Furthermore, this effect as an n -th order detection process, may be used together with a Michelson interferometer as an extremely sensitive, n -th order intensity and interferometric autocorrelator to detect any kind of very short temporal characteristic connected with the few-cycle duration.

I used a different laser system for these investigations, namely a chirped-pulse-amplified (CPA) Ti:sapphire laser, with a prism-based pulse compressor delivering ~ 25 fs-long (FWHM) pulses with ~ 1.1 mJ pulse energy and a repetition rate of 1 kHz. (Details of this particular laser system were described by Sartania et al., 1997, for the first time). The central wavelength was 800 nm. The polarization of these pulses could be rotated continuously with a broadband, $\lambda/2$ wave plate. After a further pulse compression stage consisted of a Ne-filled, 1.0 m-long, 180 μm -core diameter hollow fibre under 1.5 bar gas pressure the laser pulses were further shortened to a duration of ~ 10 fs with the aid of broadband chirped mirrors. The achievable pulse length during the measurements was unfortunately limited by the

lower amplifier output due to crystal damage. Due to the fact that the bandwidth of the wave plate was insufficient for the ~ 10 fs pulses, the beam after the hollow fibre compressor could only be used in a fixed, almost perfectly linearly and horizontally polarized fashion. For the experiments I used both of the above-described outputs of the laser system.

Since pulse energies were significantly higher during these measurements a much more simple electrode pair could be used to detect the multi-photon induced photocurrent than the EMT used with the low-energy pulses. The pulses were focused at a $\sim 80^\circ$ grazing incidence angle onto a 2 mm-thick polished, chemically treated and baked polycrystalline gold surface situated in a vacuum vessel (10^{-7} mbar) together with the electron collecting electrode kept at ~ 15 kV. The thickness of the optical window of the vacuum vessel was reduced to 1.1 mm. This amount of glass was compensated for by inserting an extra chirped mirror in the beam path. From the 4.6 eV work function value of gold and the 1.55 eV laser photon energy value follows that $n = [W/h\nu + 1] = 3$, where W indicates the work function of gold and square brackets stand for the closest integer less than the argument.

In the first experiment to determine the order of nonlinearity of the effect (i. e., the value n) the $j = f(I_p)$ intensity dependence was measured, similarly to the measurement in Section 3.3 (Fig. 16). The total electric field vector E_0 of the light was close to perpendicular to the cathode surface: $E_\perp \approx E_0$. Plotting the measured average monitor power of the pulse train and MSPE current (j) pairs in a log-log coordinate system, the slope of the fitted curve obtained gives the power value n (Fig. 19, inset). The laser intensity variation was limited to the $10^{10} - 10^{12}$ W/cm² range (to avoid both the eventual space charge saturation and the tunnel effect) and was realized by Fresnel reflecting a portion of the beam off 5- μ m-thin pellicle beam splitters. This way I avoided any kind of additional dispersive, diffraction or pointing instability artefacts upon intensity variation that would render subsequent measurement data points incomparable. It can be seen that in this intensity range the predicted $j \propto I_p^n$ multi-photon relation holds with an $n \sim 3$ measured slope value for both the ~ 25 -fs and the ~ 10 -fs laser pulses, as theoretically predicted (Keldysh, 1965; Bunkin and Fedorov, 1965).

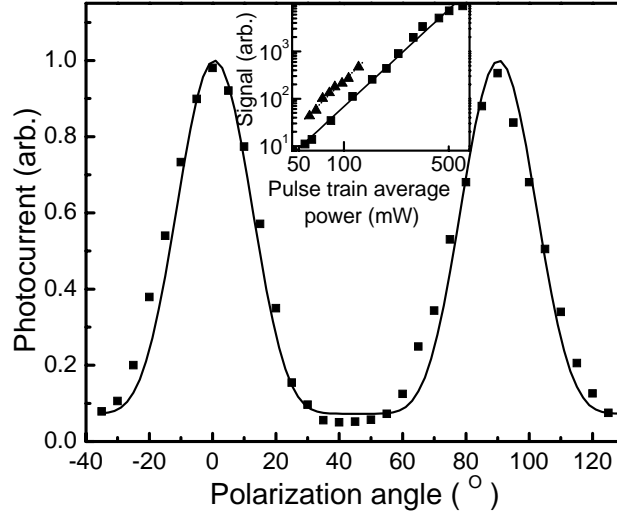


Figure 19. MSPE photocurrent as a function of the polarization angle with respect to the E -field of a ‘P’-polarized beam. The fit is a \cos^6 function. For the measurement ~ 25 fs pulses were utilized. The inset shows the intensity dependence of the MSPE photocurrent measured with ~ 25 fs-long (squares) and ~ 10 fs-long (triangles) laser pulses plotted on a log-log scale, in arbitrary units. The slopes of the fits to the measured points correspond to orders of nonlinearity of 2.9 ± 0.1 , and 3.1 ± 0.2 , respectively. The relative position of the two data sets is not meaningful, since different focussing geometries were used.

Experimental investigations have also been carried out on the polarization dependence of the photoemission. Considering that the MSPE is a function of E_{\perp} only, while the other possible processes (bulk photoeffect and the eventual thermoemission) depend on the square of the total electric field amplitude $|E_0|^2$, the polarization dependence is an extremely decisive phenomenon to distinguish between pure MSPE and other types of processes. The polarization measurements were performed by inserting and rotating a $\lambda/2$ wave plate in the train of 25 fs-long pulses. The polarization direction of the incident light is determined by the angle φ between the plane of polarization of the electric vector and the normal to the plane of the cathode surface. The experimental results are presented in Fig. 19.

It can be seen that the measured photocurrent j depends on E_{\perp} as theoretically predicted, i.e., $j \propto |E_0 \cos \varphi|^{2n} = E_0^6 \cos^6 \varphi$, corresponding to the conditions of the (vectorial) MSPE. The small deviation of the measured values from the theoretical

ones may be attributed to the fact that the light was not perfectly linearly, but slightly elliptically polarized.

The third part of this experimental campaign was devoted to the investigation of the time behaviour of the MSPE. Ultrafast intense laser pulses may induce an $h\nu$ laser photon-separated energy level structure extending over the metallic potential well and the continuum (Georges 1995 and 1996). This structure is the basis of the ATI type electron emission and HHG applied for the case of solids (Faisal and Kaminski 1997 and 1998). While both ATI and HHG have been extensively investigated, the problem of ultrafast dynamic formation of an $h\nu$ -structured step-like Fermi-distribution (Schwengelbeck et al., 2002), furthermore the decay of the vacuum levels have been explored to a less extent and only for the $n = 2$ case (Schoenlein et al., 1998; Weida et al., 2000; Hattori et al., 2000). In these references calculation and experiment show the appearances of short and long decay times manifesting in the lengthened wings of the second order interferometric autocorrelation distributions at excitation of metal surfaces and bulk (for $n = 2$).

The above-described beam of 10-fs pulses was sent into a Michelson interferometer the output of which was used to induce the MSPE process from a gold electrode enclosed in a sealed and evacuated glass tube. The intensity was restricted to the perturbative regime excluding the possibility of tunnelling emission. The emitted electrons were collected by an anode to which 15 kV extraction voltage was applied. Since the electron emission is a third-order process and according to the simplified Sommerfeld-model for metallic electrons the emitted charge should show a $j \propto |E_{\perp}|^{2n}$ dependence on the field component perpendicular to the surface one can record third-order autocorrelation curves by measuring the signal for each delay between the two interfering pulses.

Therefore, I also carried out a measurement using the gold cathode at the exit of a Michelson-interferometer as a multi-photon ($n = 3$) detector at a grazing incidence again. Using the 10-fs laser pulses I have taken interferometric autocorrelation (IACF) curves. A typical distribution can be seen in Fig. 20, where the insets show the conventional second harmonic IACF of the laser pulse and its spectrum for reference. Using these data the polynomial spectral phase of the pulse could be roughly reconstructed by fitting the coefficients of second-, third- and fourth-order phase terms. The contours of the autocorrelation trace that was

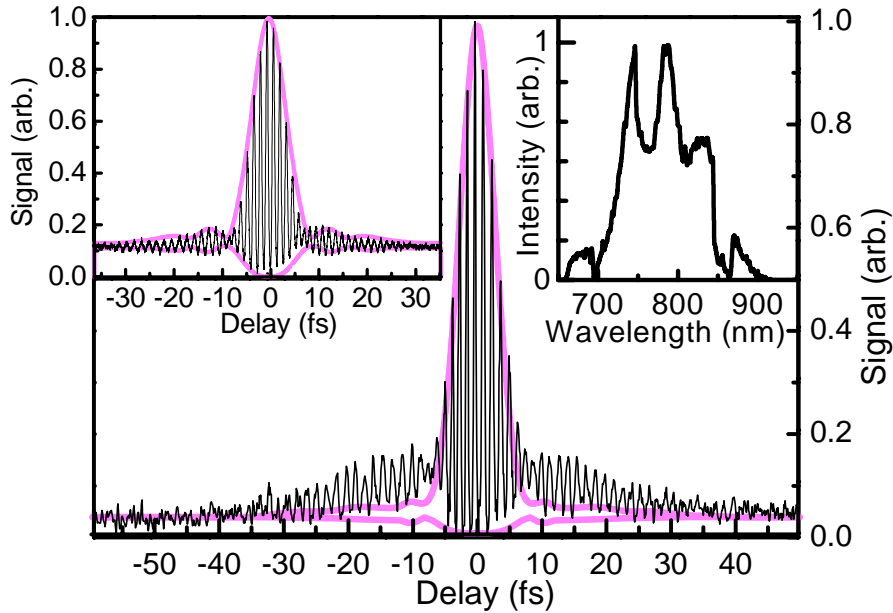


Figure 20. Measured third order autocorrelation curve of a 9.5-fs laser pulse using the gold surface. The thick contour line corresponds to the roughly reconstructed envelope of the third order interferometric autocorrelation function of the pulse by fitting a polynomial spectral phase function. The left-hand-side inset shows a pulse diagnostic measurement carried out with a conventional second harmonic autocorrelator and the reconstructed envelope of the second order autocorrelation curve using the polynomial spectral phase function. The right-hand-side inset shows the spectrum of the pulse.

calculated using the measured spectral intensity and the reconstructed spectral phase data match well those of the measured second-order autocorrelation curve and indicate uncompensated higher order dispersion in the system (left-hand-side inset in Fig. 20). The fit of the reconstructed IACF to the measured one is surprisingly good, in spite of the relatively low number of fit parameters (3) used. This suggests some contradiction with the results of Section 2.3 at first sight, where sophisticated optimization algorithms with dozens of fit parameters had to be used to achieve a satisfactory fit. One has to consider, however, that in that case the pulse spectrum was broader by a factor of 2.5 and for a reasonable pulse reconstruction the spectral phase has to be retrieved over the full spectral domain that can almost be considered as a supercontinuum. With 10-fs pulses this spectral region is much narrower and achieving a reasonable fit was possible with less free parameters.

After these preliminary tests I measured the high order ($n = 3$) autocorrelation curve (Fig. 20), that turned out to be differing a lot from the reconstructed third-order

IACF. (The reconstruction was obviously carried out using the pulse characterization data acquired in the above manner). The most conspicuous feature is the ~ 25 fs pedestal-like lengthening in both wings. This cannot be simply explained by uncompensated higher order dispersion in the system, as one might think at first sight, but demonstrate the appearance of the decay of some of the induced energy levels of the metal. Correspondingly, the central part of the curve is also broader than expected. At sufficiently long delays though (± 50 fs), coinciding with the theoretical prediction the curves show the correct 32:1 contrast value, indicating third order MSPE from a surface with the work function of gold. These observations are in accordance with previous measurements of MSPE from other types of surfaces with longer pulses and for the $n=2$ case (Hattori et al. and Weida et al., 2000) and indicate the potential harm that ultrafast dynamics of hot electrons can do to CE phase sensitivity.

The decoherence of these intermediate electron states on the observed time scale can lead to the severe loss of the sensitivity of the MSPE electron yield to the CE phase. Instantaneous electron emission is predicted to cause a yield modulation of as much as 50 % for 5-fs pulses (Lemell et al., 2003), whereas the recently observed modulation depth was well below the percent level (Dombi et al., 2004). Based on this first measurement further investigations are needed to identify exactly the underlying physical effects, for example potential involvement of image potential states in the process or to see whether it is the polycrystalline nature of the surface that results in this distortion not predicted by recent models. The benefit these studies could bring would be the identification of an optimum material configuration that can be applied successfully if the beneficial CE phase sensitivity has to be preserved. As a next step I will study MSPE characteristics of a single-crystal gold surface with 5-fs laser pulses under ultrahigh vacuum conditions.

3.5 Discussion and outlook

The achievements presented in this chapter are based on the first observation of a CE phase sensitive laser-solid interaction. These results were gained at the same time as the waveform sensitivity of HHG was shown and together they constitute the

first-ever demonstrations of light-matter interaction processes directly sensitive to the CE phase. These findings are therefore very important from the basic research point-of-view. The benefits of inducing HHG with controlled optical waveforms in terms of attosecond science can be directly seen just by looking at the cut-off regions of the spectra generated with different waveforms, as illustrated in the Motivation section.

As for benefits in applied science these phenomena are also interesting, since they could serve as a basis for direct measurement of the CE phase (φ) as opposed to f -to- $2f$ interferometry, being sensitive to $\Delta\varphi$ only. Since there is an inherent ambiguity in phase measurement with HHG (namely, it can not make a difference between a *cosine* and a *minus cosine* waveform), it seemed that MSPE is the only candidate for such an application with the inherent symmetry breaking due to the metal surface that makes unambiguous phase determination possible in principle. The low phase contrast of this phenomenon, however, puts a curb to such practical applications. At the time of submitting this thesis no convincing arguments had been brought up as to what might cause the discrepancy between rigorous simulations (or a simple phenomenological model) and first observations I delivered. None of the mentioned contrast reducing effects whether it be of technical nature (lack of ultrahigh vacuum or surface quality) or fundamental limitations (for example, some ultrafast level dynamics) seem to explain the annoying discrepancy convincingly.

As a parallel branch of research, shortly after the first observation of CE phase dependent MSPE it turned out that ATI can be used as a high-contrast method for direct CE phase measurement resolving the ATI electrons either spatially or spectrally. Because of the high contrast it delivered and the moderate pulse energies it could be used with first applications have already appeared where the output of an amplified laser system is stabilized in this way (Liu et al., 2004). The reasons that this method was chosen instead of standard f -to- $2f$ interferometry will be illuminated in the next chapter.

4 Analysis of CE phase effects upon ultrashort pulse propagation

As soon as the generation of few-cycle pulses* with Ti:S lasers seemed within reach corresponding questions were raised both about their propagation and about light-matter interaction involving them. Even though these two class of questions can not be strictly separated (think of ultrashort pulse propagation in ionizing media), one can make a difference, for example between linear propagation of a few-cycle pulse in a dispersive medium and a high-field interaction induced by such a pulse, such as HHG. Corresponding questions can be formulated as: does the carrier-envelope decomposition of the pulse remain meaningful in this case? Respectively, the second one could be: does the slowly varying envelope approximation make sense? In this chapter I will overview the answers to these and some similar questions and I will present my results concerning the analysis of the evolution of the CE phase during linear, dispersive propagation of few-cycle pulses and its implications in terms of CE phase stabilization.

4.1 Few-cycle pulse propagation and interactions

I use the carrier-envelope description for the temporal electric field evolution of a laser pulse. The electric field can be unambiguously decomposed into a carrier wave and an envelope in the form of $E(t) = A(t)\cos(\omega_L t + \varphi)$, if one fixes ω_L as the centre of gravity of the spectral intensity distribution of the pulse. This procedure yields a reasonably smooth envelope, $A(t)$, in almost all practical cases. For a self-consistent description it is also necessary that the full width at half intensity maximum (FWHM) pulse length, τ_p , is longer than the oscillation period of the carrier wave (Brabec and Krausz, 2000). Satisfaction of this condition ensures that ω_L and $A(t)$ remain invariant to a change of φ , which is necessary for examining any phase-sensitive phenomenon. The $\tau_p > 2\pi/\omega_L$ condition is met even for the shortest

* The definition of a few-cycle pulse is somewhat arbitrary, one could say < 8 fs intensity FWHM corresponding to three oscillation cycles for Ti:S pulses.

visible laser pulses available to date (Schenkel et al., 2003 and Yamane et al., 2003), permitting an unambiguous and consistent definition of φ .

In general, φ tends to evolve on significantly shorter propagation lengths than the pulse shape. For example, for a 4-fs-long, Gaussian pulse centred at 750 nm the characteristic propagation length of CE phase evolution is about 25 μm in fused silica, upon which a pulse with $\varphi = 0$ changes into a pulse with $\varphi = \pi$. Such a small amount of dispersion does not change significantly the pulse shape even for such a short pulse. However, for ultrabroad-band pulses with τ_p approaching $T_0 = 2\pi/\omega_L$ a variation of φ may not be completely decoupled from that of $A(t)$. Implications of this will be scrutinized in Section 4.4.

If such short pulses interact with matter intuition suggests that the interaction is not governed by some quasiconstant amplitude of the oscillations any more, as suggested by the slowly varying amplitude approximation, but the actual temporal evolution of the electric field comes into play. Even in this case one can make a less limiting approximation, called the slowly evolving wave approximation by assuming that the CE phase does not change significantly upon propagation a distance equal to the wavelength (Brabec and Krausz, 2000).

A very illustrative example of a high-field interaction that is governed by the field evolution is HHG. As mentioned in the Motivation section the XUV spectrum shows a completely different shape if it is generated by a few-cycle *cosine* pulse as compared to the XUV spectrum induced by a *sine* pulse (Fig. 2). For the *sine* pulse the cut-off region is modulated due to the highest photon energies generated at two, equivalent instants of the pulse and harmonic lines are at integer odd multiples of the carrier frequency. For a few-cycle *cosine* pulse the cut-off region is smooth because no destructive interference can come about for the highest photon energies and the discrete lines are not at integer odd multiples of the carrier frequency, since XUV photons with the same energy are generated by portions of the pulse separated by $(n + 1/2)\lambda_0$ (where n is an integer), as opposed to a few-cycle *sine* pulse or a sufficiently long pulse with any CE phase.

4.2 Drawbacks of f -to- $2f$ interferometry

The measurements presented in Sections 2.4 and 3.3 revealed that *both* $L_{f\text{-to-}2f}$ and L_{MSPE} agree, within the experimental accuracy, with the dephasing length, L_{deph} . This would suggest that both the f -to- $2f$ signal and the photoemission signal are, in principle, suitable for measuring φ in the laser pulse train. In general, however, this is not true. In fact, for $L_{f\text{-to-}2f}$ a simple analysis yields $L_{f\text{-to-}2f} = |\Delta n / \Delta \lambda|^{-1} / 2$, where $\Delta n / \Delta \lambda = [n(\lambda_h) - n(\lambda_l)] / (\lambda_h - \lambda_l) = -[n(\lambda_h) - n(2\lambda_h)] / \lambda_h$ and n is the refractive index of the propagation medium. (λ_h indicates the wavelength of higher energy photons in the green wing of the fundamental spectrum interfering with the frequency-doubled signal having originally a wavelength of λ_l .) However, for the dephasing length one obtains $L_{\text{deph}} \approx |dn/d\lambda|^{-1} / 2$, where $dn/d\lambda$ is the first derivative of $n(\lambda)$ at the carrier wavelength λ_0 (Brabec and Krausz, 2000).

From these analytic expressions it becomes clear that $L_{f\text{-to-}2f} = L_{\text{deph}}$ holds irrespective of λ_0 if and only if $n(\lambda)$ is a linear function of λ , i.e. in the absence of

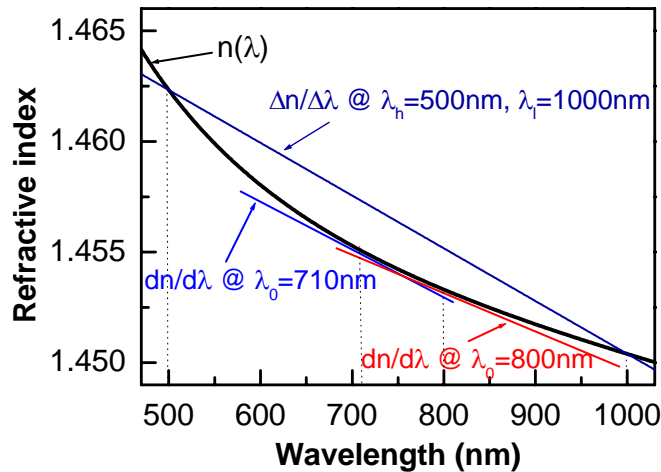


Figure 21. Refractive index of fused silica versus wavelength and the quantities relevant to the phase change of the f -to- $2f$ beat signal and the shift of the carrier-envelope phase with a change in the propagation length through this material. See text for further explanations.

dispersion. Figure 21 reveals that in a dispersive medium these two quantities (the slope of the respective light and dark blue lines) are only accidentally equal to each other for a specific choice of λ_0 and/or for a special spectral distribution, which happens to apply in our case for λ_0 near 690 nm (Yakovlev, Dombi et al., 2003). By contrast, a carrier wavelength of $\lambda_0 = 800$ nm would imply a dephasing length, L_{deph} that deviates by more than 35% from $L_{f\text{-to-}2f}$ at $\lambda_h = 500$ nm in fused silica, i.e. the slope of the red curve in Fig. 21 appreciably deviates from that of the dark blue.

This has important implications if one intends to stabilize the phase precisely for an extreme non-linear optical experiment carried out with amplified laser beams. Since dispersive path length fluctuations in a complex, multiple-stage amplifier system can easily add up to a value comparable to the dephasing length a phase stabilization system based on the $f\text{-to-}2f$ technique will improperly compensate for any phase drift or jitter and perfect on-target phase stabilization will therefore not be achieved. It is thus necessary to carry out *direct* phase measurement, preferably with a small portion of the beam and preferably using a compact device as demonstrated in Chapter 3.

The fact that the $f\text{-to-}2f$ technique is unable to measure φ reliably in the presence of dispersion prompts the important question whether the application of this technique to controlling the evolution of the carrier-envelope phase in a cw mode-locked laser, which always contains dispersive elements, achieves the desired effect, namely control of the carrier-envelope phase evolution. The answer is *yes*. This is because intracavity dispersion is not permitted to modify the circulating pulse from one round-trip to the next. In the stationary case of cw mode locking, the femtosecond laser pulse precisely reproduces itself in the output pulse train (apart from a possible shift in the carrier-envelope phase) owing to a subtle interplay between non-linear processes and dispersive effects. Because the pulse is always the same except for a shift in its carrier-envelope phase ($\Delta\varphi$), the $f\text{-to-}2f$ technique can reliably measure this quantity and stabilize f_{ceo} . In contrast to this, propagation through dispersive elements outside the laser cavity leads to modification of several pulse properties (rather than only φ) simultaneously. Contrary to the difficulties with the $f\text{-to-}2f$ technique, L_{MSPE} is found to be equal to L_{deph} with a good accuracy in simulations irrespective of the specific choice of the carrier wavelength. This finding backs the simple intuitive arguments presented above.

4.3 Effects of linear pulse propagation on the CE phase

The validity of the approximation $L_{\text{deph}} \approx |dn/d\lambda|^{-1}/2$ is also worth a closer look. I computed the carrier-envelope phase shift of a Gaussian pulse by evaluating propagation equations in a dispersive medium and compared the results given by the approximation formula. The difference between these two quantities is depicted in Figure 22 as a function of the propagation distance (in units of the dephasing length in fused silica). For a Gaussian pulse three curves were calculated, for pulses having an intensity FWHM duration of 4 fs, 6 fs and 10 fs. As expected, for a 4-fs pulse the dephasing length approximation breaks down, whereas already a 6-fs Gaussian pulse is “long enough” (and not so much different from a 10-fs-one from this point of view) for its envelope not to change too much during propagation, preserving the validity of the approximation.

Apart from the pulse length the actual pulse shape can also influence carrier-envelope phase relations upon propagation. The same calculation was made for the

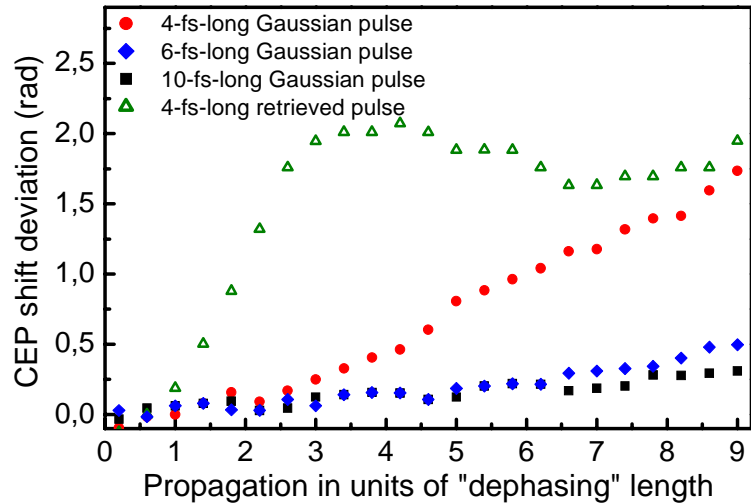


Figure 22. Deviation of the accurate CE phase shift value (taking dispersive pulse distortion into account) from the value calculated according to the dephasing length approximation. Results for pulses with Gaussian envelopes having different pulse lengths are depicted, as well as for a more realistic pulse envelope retrieved from our pulse diagnostic system (Yakovlev, Dombi et al., 2003). The central wavelength is 710 nm in all four cases.

pulse shapes retrieved from measurements with our pulse diagnostic system (Yakovlev, Dombi et al., 2003). My study reveals that the above approximation fails even more for a pulse with a complex spectral and temporal shape (Figure 22). The irregularities observed for the retrieved pulse shape (for example, the strong deviation in the first part of the curve) are not just limited to its CE phase behaviour since the dependence of the pulse length is just as irregular. These can be explained by the fact that the actual ultrashort 4-fs pulse with its highly structured spectrum and temporal envelope will suffer significant envelope distortion during propagation in a relatively small amount of dispersive material. After about 70 μm of propagation this difference will stop growing probably owing to the fact that the pulse is now chirped and therefore temporally stretched enough for its envelope not to be affected so much by dispersion. In this case the dephasing length value will provide an acceptable approximation of the CE phase slip, represented by the close-to-horizontal part of the curve.

These simulations back the above conclusion that a direct phase measurement technique is required to stabilize the CE phase against extracavity jitter. Since optical path length fluctuations in a high-power laser system can easily attain the dephasing length, it is of utmost importance to use a method of phase stabilization that is directly sensitive to the relative timing of the electric field oscillation to the pulse envelope peak. Sampling just the spectral wings of the beam, as the f -to- $2f$ technique does, does not provide sufficiently accurate information on the shift of the carrier-envelope phase caused by some change in the optical path length through components outside the phase-stabilized oscillator. This conclusion is also valid for amplified laser systems delivering 5-7 fs pulses typically used for attosecond experiments, since unless one has well-behaved Gaussian pulses the effect of the imperfectness of the f -to- $2f$ phase stabilization will be noticeable, as already experimentally observed elsewhere (Liu et al., 2004).

4.4 Direct CE phase stabilization

Since both the arguments presented in Section 4.2 and 4.3 prompt for direct phase-stabilization to achieve on-target waveform stability one has to consider a scheme potentially suitable for such a purpose. Such a scheme should include a CE

phase measurement stage and feedback control. Building on other researchers' results already mentioned in Section 3.1 and the results of my investigations concerning MSPE described in Chapter 3, one can overview and summarize all CE phase-sensitive physical phenomena with respect to their usability for direct phase stabilization.

The most important required characteristics for CE phase measurement can be seen in the heading of Table 1. The device should have a high contrast and it should be compact and easy-to-operate. It is typically with few-cycle pulses and high-field interactions, where CE phase issues become crucial. Typical workhorse laser systems in this parameter regime deliver sub-mJ pulse energies. CE phase stabilization should be carried out with a fraction of the output of such systems, therefore maximum allowed pulse energies that can be used for such a purpose lie in the $<10 \dots 100 \mu\text{J}$ range. Single-shot operability is, of course, of utmost importance with laser systems with kHz repetition rates and below.

process	contrast	compactness	pulse energy needed	single shot	trivial calibration	ambiguity	tested in practice	references
HHG	+	--	high	+	+	yes	yes	Baltuška et al., 2003
MSPE	-	+	v. low	+	-	none	yes	Lemell et al., 2003 Dombi et al., 2004
ATI	+	-	low	+	+	none	yes	Paulus et al., 2001, 2003
semicond.	-	++	v. low	+	-	none	yes	Fortier et al., 2004
(surface) harm.	(++)	++	low	+	-	none	no	Mehendale et al., 2000 Varró, 2004
NSDI	-	--	low	-	-	none	yes	Liu et al., 2004

Table 1. Overview and evaluation of light-matter interaction processes potentially applicable for direct CE phase measurement. + and ++ mean relaxed requirements or positive features from the given point-of-view. Symbols in brackets mean experimentally not yet confirmed features. For further explanation see text and references.

Calibrating the CE phase measurement method also raises some interesting specific issues. The cross-calibration of any two of these CE phase measurement methods is very difficult to realize. For this, recall that, for example, extra propagation of $\sim 10 \mu\text{m}$ in fused silica makes a *cosine*-pulse out of a *sine*-pulse. If

two methods were to be cross-calibrated the same beam has to be used, and split for use in two beamlines. In case, for example, of a dielectric beam splitter its thickness would have to be known to within an accuracy of, say, $2\ \mu\text{m}$ for a reasonable CE phase calibration accuracy. The path lengths of these beamlines would have to be made equal to within an accuracy that cannot be realized either unless the beam propagates only in vacuum after the beamsplitter. Even in this case careful target focusing design would be a must to avoid CE phase artefacts due to the Gouy phase shift near focus (Lindner et al., 2004). Since cross-calibration is thus practically excluded, one needs a method having a straightforward calibration that can be derived from simple principles.

The issue of CE phase measurement ambiguity mostly appears either due to the centrosymmetric nature of the medium, as with HHG or the spatially unresolved electron detection. In practice this means that the CE phase measurement apparatus cannot make a difference between e.g. a *cosine* and a *minus cosine* pulse. This problem is only present with HHG, in case of surfaces the 'P'-polarized grazing incidence geometry breaks the symmetry, in case of ATI the spatially resolved electron detection. The different, observed and/or predicted CE phase sensitive phenomena are listed in the first column of Table 1. The table gives a rough evaluation of all of them for potential direct phase measurement applications from the above-listed points-of-view.

For completeness two rows have to be added to the table additionally to those phenomena already mentioned more or less in this thesis. One is a solid-state-based method, drawing on controlling the injected current in a low-temperature grown GaAs sample (Fortier et al., 2004). It seems that it is only the solid-state nature of this approach that could make it attractive, since both its low contrast and not trivial calibration mean severe disadvantages. Very recently non-sequential double ionization (NSDI) was also examined using controlled optical waveforms and phase effects were found indeed, but this phenomenon is definitely something, which can be interesting only for basic research due to the sophisticated detection required.

It was already mentioned that few-cycle pulse applications with relativistic intensities will also probably require CE phase control technologies. Current laser systems are quite far from this parameter regime and theoretical studies have not been carried out for such interactions, either. Therefore, I cannot go into details about it in this overview section either.

As a summary, one can say that at the time of the submission of this thesis there is no standard solution that could be used for direct CE phase stabilization of few-cycle CPA laser output beams as a substitute to f -to- $2f$ interferometry. There are promising alternatives, however, each method suggested has at least one drawback spoiling its attractiveness. Direct phase stabilization would bring benefits especially for experiments in basic research, future attosecond or XUV spectroscopic, broadband pump-probe etc. applications, where long acquisition times are required.

5 Conclusions and outlook

Investigating extreme nonlinear optical interactions induced by few-cycle waveforms is a rapidly evolving field of research which earned wide scientific and public attention due to its most imagination-catching subclass, attosecond science. This field, the real birth of which is not even four years ago (if one dates it at the first confirmed generation of isolated attosecond pulses) is continuously expanding and holds promise of allowing insight into the fastest processes in nature one could ever take a “time-resolved look” at. Related technology is mature enough to increase the magnification of this best “temporal magnifying glass” mankind ever had by an order of magnitude in the near future.

Since controlled optical waveforms are at the heart of reproducible attosecond pulse generation, the technology related to this will preserve its importance for years to come. Using attosecond XUV pulses together with phase-controlled optical waves allows the investigation of inner-shell dynamics of atomic electrons. This could be very important, for example, for identifying and characterizing those processes that could be crucial for X-ray laser development. Related to the improvement of CE phase stabilization I pursued the goal of directly measuring the CE phase of laser pulses, which necessitates a suitable laser system together with pulse and phase diagnostics and a highly nonlinear light-matter interaction for CE phase measurement. I reported on the construction of such a laser, which delivered one of the shortest optical pulses of its time, as well as controlled optical waveforms available for nonlinear optical experiments with a high repetition rate. These features make this laser system unique, since it allows access to such an intermediate parameter regime for which oscillators do not usually deliver enough power and for which the employment of amplified laser systems would be overkill. Moreover, acquisition times can be substantially reduced with a MHz laser system.

The specific laser-solid interaction that I investigated was photoelectron emission from a metal surface, known for almost 120 years. This showed, however, a new face when instead of simply continuous light or light pulses, CE phase stabilized ultrashort pulses were used to induce the effect. It seemed for a while that this effect would be the best candidate for single-shot direct CE phase measurement, but due to its low contrast it lost its attractiveness. It remains an open question and challenge for

future theoretical and experimental investigations in basic research why the observed sensitivity is much lower than the predicted one (supported by a sophisticated and a simple model, too). However, the questions raised during this research provided answers especially in terms of the CE phase stabilization of amplified laser systems, without which long acquisition time waveform-sensitive measurements (such as that of non-sequential double ionization, Liu et al., 2004) would be impossible.

The application of waveform control technology to laser systems with even higher brightness would lead to a field completely unexplored, namely that of CE-phase sensitive relativistic interactions. Few-cycle laser pulses and controlled optical waveforms might bring advantages in laser wake-field acceleration of electrons and protons and might open a new era in particle acceleration. These possibilities have not been explored in depth, yet (not even theoretically), nevertheless laser systems under construction should reach unprecedented parameter regimes in a couple of years.

Whether these improvements related to few-cycle laser pulses and their waveform control together with the technologies growing out of this research (such as attosecond spectroscopy and metrology) will bring the availability of table-top laser-driven particle accelerators or X-ray lasers will hopefully be answered in the future.

Abbreviations

ATI	above threshold ionization
CE	carrier-envelope
CEO	carrier-envelope offset
CM	chirped mirror
CPA	chirped pulse amplification
EMT	electron multiplier tube
FROG	frequency-resolved optical gating
FWHM	full width at half maximum
GDD	group delay dispersion
HHG	high harmonic generation
IACF	interferometric autocorrelation function
KLM	Kerr-lens mode-locked
MDC	mirror dispersion-controlled
MSPE	multi-photon-induced surface photoelectron emission
NSDI	non-sequential double ionization
PCF	photonic crystal fibre, also called as microstructured fibre
PICASO	phase and intensity from correlation and spectrum only
SC	supercontinuum
SH	second harmonic
SPIDER	spectral phase interferometry for direct electric field reconstruction
SPM	self phase modulation
TFI	tilted front interface
Ti:S	titanium-doped sapphire
TOD	third order dispersion
XUV	extreme ultraviolet

Bibliography

- Agostini, P. and L. DiMauro, 2004, *Rep. Prog. Phys.* **67**, 813.
- Agostini, P., F. Fabre, G. Mainfray, G. Petite, N. Rahman, 1979, *Phys. Rev. Lett.* **42**, 1127.
- Ames, J. N., S. Ghosh, R.S. Windeler, A.L. Gaeta, S.T. Cundiff, 2003, *Appl. Phys. B* **77**, 279.
- Apolonski, A., P. Dombi, G. G. Paulus, M. Kakehata, R. Holzwarth, Th. Udem, Ch. Lemell, K. Torizuka, J. Burgdörfer, T. W. Hänsch, F. Krausz, 2004, *Phys. Rev. Lett.* **92**, 073902.
- Apolonski, A., A. Poppe, G. Tempea, Ch. Spielmann, T. Udem, R. Holzwarth, T.W. Hänsch, F. Krausz, 2000, *Phys. Rev. Lett.* **85**, 740.
- Baltuška, A., T. Fuji, T. Kobayashi, 2002, *Phys. Rev. Lett.* **88**, 133901.
- Baltuška, A., Th. Udem, M. Uiberacker, M. Hentschel, E. Goulielmakis, Ch. Gohle, R. Holzwarth, V. S. Yakovlev, A. Scrinzi, T. W. Hänsch, F. Krausz, 2003, *Nature* **421**, 611.
- Boyd, R. W., “*Nonlinear Optics*”, 1997, Academic Press, San Diego, USA.
- Brabec, Th. and F. Krausz, 2000, *Rev. Mod. Phys.* **72**, 545.
- Bunkin, F. V., and M.V. Fedorov, 1965, *Sov. Phys. JETP* **21**, 896.
- Christov, I. P., 2000, *Appl. Phys. B* **70**, 459.
- Chung, J. and A. Weiner, 2001, *IEEE J. Sel. Top. Quantum Electron.* **7**, 656.
- Corkum, P. B., 1993, *Phys. Rev. Lett.* **71**, 1994.
- Cormier, E. and P. Lambropoulos, 1998, *Eur. Phys. J. D* **2**, 15.
- Cundiff, S. T., J. Ye, 2003, *Rev. Mod. Phys.* **75**, 325.
- Dombi, P., A. Apolonski, Ch. Lemell, G. G. Paulus, M. Kakehata, R. Holzwarth, Th. Udem, K. Torizuka, J. Burgdörfer, T. W. Hänsch, and F. Krausz, 2004, *New J. Phys.* **6**, 39.
- Dombi, P., F. Krausz, Gy. Farkas, 2005, in preparation.
- Faisal, F. H. M. and J. Z. Kaminski, 1997, *Phys. Rev. A* **56**, 748.
- Faisal, F. H. M. and J. Z. Kaminski, 1998, *Phys. Rev. A* **58**, R19.
- Farkas, Gy. and Cs. Tóth, 1992, *Phys. Lett. A* **168**, 447.
- Faure J., Y. Glinec, A. Pukhov, S. Kiselev, S. Gordienko, E. Lefebvre, J.-P. Rousseau, F. Burgy, V. Malka 2004, *Nature* **431**, 541.

- Fortier T. M., J. Ye, S. T. Cundiff, R. S. Windeler, 2002a, *Opt. Lett.* **27**, 1436.
- Fortier, T. M., D. J. Jones, J. Ye, S. T. Cundiff, R. S. Windeler, 2002b, *Opt. Lett.* **27**, 445.
- Fortier, T. M., P. A. Roos, D. J. Jones, S. T. Cundiff, R. D. R. Bhat, J. E. Sipe, 2004, *Phys. Rev. Lett.* **92**, 147403.
- Geddes, C. G. R., C. Toth, J. van Tilborg, E. Esarey, C. B. Schroeder, D. Bruhwiler, C. Nieter, J. Cary, W. P. Leemans, 2004, *Nature* **431**, 538.
- Georges, A. T., 1995, *Phys. Rev. B* **51**, 13735.
- Georges, A. T., 1996, *Phys. Rev. A* **54**, 2412.
- Hattori, T., Y. Kawashima, M. Daikoku, H. Inouye and H. Nakatsuka, 2000, *Jpn. J. Appl. Phys.* **39**, 4793.
- Helbing, F. W., G. Steinmeyer, U. Keller, 2003, *Laser Phys.* **4**, 644.
- Helbing, F. W., G. Steinmeyer, U. Keller, R.S. Windeler, J. Stenger, H.R. Telle, 2002, *Opt. Lett.* **27**, 194.
- Hentschel, M., R. Kienberger, Ch. Spielmann, G. A. Reider, N. Milosevic, T. Brabec, P. Corkum, U. Heinzmann, M. Drescher, F. Krausz, 2001, *Nature* **414**, 509.
- Iaconis, C. and I. A. Walmsley, 1999, *IEEE J. Quant.El.* **35**, 501.
- Jones, D. J., S. A. Diddams, J. K. Ranka, A. Stentz, R. S. Windeler, J. L. Hall, S. T. Cundiff, 2000, *Science* **288**, 635.
- Kakehata, M., H. Takada, Y. Kobayashi, K. Torizuka, Y. Fujihira, T. Homma, H. Takhashi, 2001, *Opt. Lett.* **26**, 1436.
- Kalashnikov, V., P. Dombi, T. Fuji, W. Wadsworth, J. C. Knight, P. S. J. Russell, R. S. Windeler, A. Apolonski, 2003, *Appl. Phys. B.* **77**, 319.
- Keldysh, L.V., 1965, *Sov. Phys. JETP* **20**, 1307.
- Lemell, Ch., X.-M. Tong, F. Krausz, J. Burgdörfer, 2003, *Phys. Rev. Lett.* **90**, 076403.
- Lewenstein, M., Ph. Balcou, M. Yu. Ivanov, Anne L'Huillier, P. B. Corkum, 1994, *Phys. Rev. A* **49**, 2117.
- Lindner, F., G. G. Paulus, H. Walther, A. Baltuska, E. Goulielmakis, M. Lezius, F. Krausz, 2004, *Phys. Rev. Lett.* **92**, 113001.
- Liu, X., H. Rottke, E. Eremina, W. Sandner, E. Goulielmakis, K. O'Keeffe, M. Lezius, F. Krausz, F. Lindner, M. G. Schätzel, G. G. Paulus, H. Walther, 2004, *Phys. Rev. Lett.* **93**, 263001.

- Mangles, S. P. D., C. D. Murphy, Z. Najmudin, A. G. R. Thomas, J. L. Collier, A. E. Dangor, E. J. Divall, P. S. Foster, J. G. Gallacher, C. J. Hooker, D. A. Jaroszynski, A. J. Langley, W. B. Mori, P. A. Norreys, F. S. Tsung, R. Viskup, B. R. Walton, K. Krushelnick 2004, *Nature* **431**, 535.
- Mehendale, M., S. A. Mitchell, J.-P. Likforman, D. M. Villeneuve, P. B. Corkum, 2000, *Opt. Lett.* **25**, 1672.
- Mittleman, D. M., R. H. Jacobsen, M. C. Nuss, 1996, *IEEE J. Sel. Top. Quant. El.* **2**, 679.
- Mücke, O. D., T. Tritschler, M. Wegener, U. Morgner, F. X. Kärtner, 2002, *Opt. Lett.* **27**, 2127.
- Naganuma, K., K. Mogi, H. Yamada, 1989, *IEEE J. Quantum Electron.* **QE-25**, 1225.
- Nicholson, J. W. and W. Rudolph, 2002, *J. Opt. Soc. Am. B* **19**, 330.
- Nicholson, J. W., J. Jasapara, W. Rudolph, F.G. Omenetto, A.J. Taylor, 1999, *Opt. Lett.* **24**, 1774.
- O’Keefe, K., P. Jöchl, H. Drexel, V. Grill, F. Krausz, M. Lezius, 2004, *Appl. Phys. B* **78**, 583.
- Paulus, G. G., F. Grasbon, H. Walther, P. Villorosi, M. Nisoli, S. Stagira, E. Priori, S. De Silvestri, 2001, *Nature* **414**, 182.
- Paulus, G. G., F. Lindner, H. Walther, A. Baltuska, E. Goulielmakis, M. Lezius, F. Krausz, 2003, *Phys. Rev. Lett.* **91**, 253004.
- Poppe, A., R. Holzwarth, A. Apolonski, G. Tempea, Ch. Spielmann, T.W. Hänsch, F. Krausz, 2001, *Appl. Phys. B* **72**, 373.
- Pukhov, A. and J. Meyer-ter-Vehn, 2002, *Appl. Phys. B* **74**, 355.
- Reichert, J., R. Holzwarth, Th. Udem, and T.W. Hänsch, 1999, *Opt. Comm.* **172**, 59.
- Russell P., 2003, *Science* **299**, 358.
- Sartania, S., Z. Cheng, M. Lenzner, G. Tempea, Ch. Spielmann, F. Krausz and K. Ferencz, 1997, *Opt. Lett.* **22**, 1562.
- Schenkel, B., J. Biegert, U. Keller, C. Vozzi, M. Nisoli, G. Sansone, S. Stagira, S. De Silvestri, O. Svelto, 2003, *Opt. Lett.* **28**, 1987.
- Schnatz, H., B. Lipphardt, J. Helmcke, F. Riehle, and G. Zinner, 1996, *Phys. Rev. Lett.* **76**, 18.
- Schnürer, M., Z. Cheng, M. Hentschel, F. Krausz, T. Wilhein, D. Hambach, G. Schmahl, M. Drescher, Y. Lim, U. Heinzmann, 1998, *Phys. Rev. Lett.* **80**, 3236.

- Schoenlein, R. W., J. G. Fujimoto, G. L. Eesley and T. W. Capehart, 1998, *Phys. Rev. Lett.* **61**, 2596.
- Schwengelbeck, U., L. Plaja, E. C. Jarque, L. Roso, S. Varró and Gy. Farkas, 2002, *J. Phys. B* **35**, L181.
- Shen, Y. R., “*The principles of nonlinear optics*”, 1984, Wiley, New York, USA.
- Siegman, A. E., “*Lasers*”, 1986, University Science Books, Mill Valley, California, USA.
- Telle, H. R., G. Steinmeyer, A. E. Dunlop, J. Stenger, D. H. Sutter, U. Keller, 1999, *Appl. Phys. B* **69**, 327.
- Tempea, G., V. Yakovlev, B. Bacovic, F. Krausz, K. Ferencz, 2001, *J. Opt. Soc. Am. B* **18**, 1747.
- Trebino, R., K. W. DeLong, D. N. Fittinghoff, J. N. Sweetser, M. A. Krumbügel, B. A. Richman, D. J. Kane, 1997, *Rev. Sci. Instr.* **68**, 3277.
- Varró, S., 2004, *Las. Phys. Lett.* **1**, 42.
- Weida, M.J., S. Ogawa, H. Nagano and H. Petek, 2000, *J. Opt. Soc. Am. B* **17**, 1443.
- Winter, HP., *Phys. Reports* **367**, 387 (2002).
- Witte, S., R. T. Zinkstok, W. Hogervorst, K. S. E. Eikema, 2004, *Appl. Phys. B* **78**, 5.
- Xu, L., Ch. Spielmann, A. Poppe, T. Brabec, F. Krausz, T. W. Hänsch, 1996, *Opt. Lett.* **21**, 2008.
- Yakovlev, V., P. Dombi, G. Tempea, Ch. Lemell, J. Burgdörfer, Th. Udem, A. Apolonski, 2003, *Appl. Phys. B* **76**, 329.
- Yamane, K., Z. Zhang, K. Oka, R. Morita, M. Yamashita, A. Suguro, 2003, *Opt. Lett.* **28**, 2258.
- Yudin, G. L., M. Yu. Ivanov, 2001, *Phys. Rev. A* **64**, 013409.
- Zewail, A., 2000, *J. Phys. Chem. A* **104**, 5660.

Full publication list of the author

Journal Publications

- [1] I. N. Ross, C. J. Hooker, **P. Dombi**, “Efficient generation of large diffraction gratings using a grating interferometer”, *Appl. Opt.* **40**, 6153-6156 (2001).
- [2] K. Osvay, **P. Dombi**, A. P. Kovács, Z. Bor, “Fine tuning of the higher-order dispersion of a prismatic pulse compressor”, *Appl. Phys. B* **75**, 649-654 (2002).
- [3] V. S. Yakovlev, **P. Dombi**, G. Tempea, C. Lemell, J. Burgdörfer, T. Udem, A. Apolonski, “Phase-stabilized 4-fs pulses at the full oscillator repetition rate for a photoemission experiment”, *Appl. Phys. B* **76**, 329-332 (2003).
- [4] V. L. Kalashnikov, **P. Dombi**, T. Fuji, W. J. Wadsworth, J. C. Knight, P. S. J. Russell, R. S. Windeler, A. Apolonski, “Maximization of supercontinua in photonic crystal fibers by using double pulses and polarization effects” *Appl. Phys. B* **77**, 319-324 (2003).
- [5] A. Apolonski, **P. Dombi**, G. G. Paulus, M. Kakehata, R. Holzwarth, Th. Udem, Ch. Lemell, K. Torizuka, J. Burgdörfer, T. W. Hänsch, F. Krausz, „Observation of light-phase-sensitive photoemission from a metal“ *Phys. Rev. Lett.* **92**, 073902 (2004).
- [6] **P. Dombi**, A. Apolonski, Ch. Lemell, G.G. Paulus, M. Kakehata, R. Holzwarth, Th. Udem, K. Torizuka, J. Burgdörfer, T. W. Hänsch, F. Krausz, „Direct measurement and analysis of the carrier-envelope phase in light pulses approaching the single-cycle regime“, *New J. Phys.* **6**, 39 (2004).
- [7] **P. Dombi**, A. Apolonski, F. Krausz, “Photoelectrons measuring the phase of light” EuroPhysics News, July/August issue (2004), invited.
- [8] F. Légaré, Kevin F. Lee, I. V. Litvinyuk, P. W. Dooley, S. S. Wesolowski, P. R. Bunker, **P. Dombi**, F. Krausz, A. D. Bandrauk, D. M. Villeneuve, P. B. Corkum, “Laser Coulomb explosion imaging of small molecules” *Phys. Rev. A* **71**, 013415 (2005).
- [9] **P. Dombi**, F. Krausz, Gy. Farkas, “Ultrafast dynamics of multiphoton photoemission and carrier-envelope phase sensitivity”, in preparation (2005).

Conference Proceedings Books

- [10] K. Osvay, **P. Dombi**, A.P. Kovács, J. Klebniczki, G. Kurdi, Z. Bor, “Tuneable third order dispersion of a prismatic pulse compressor”, Ultrafast Phenomena XII Proceedings, p. 168-170, Springer Verlag (2001).
- [11] **P. Dombi**, A. Apolonski, G. G. Paulus, M. Kakehata, R. Holzwarth, Th. Udem, Ch. Lemell, J. Burgdörfer, T. W. Hänsch and F. Krausz, “Solid-state carrier-envelope phase detector” Ultrafast Optics IV Proceedings, p. 185-191, Springer Verlag (2004).

[12] A. Fuerbach, A. Fernandez, T. Fuji, H. Mayer, **P. Dombi**, F. Krausz, A. Apolonski, „*Generation of ultra-broadband high energy pulses without external amplification*” Ultrafast Phenomena XIV Proceedings, to appear in 2005.

Other Conference Contributions

[13] **P. Dombi**, I.N. Ross, C.J. Hooker, Z. Bakonyi, „*Large Holographic Grating Production Using a Grating Interferometer*”, Quantum Electronics and Photonics Conference 14, Manchester, UK, p. 44 (1999).

[14] **P. Dombi**, K. Osvay, A. P. Kovács, J. Klebniczki, G. Kurdi, Z. Bor, “*Tuneable Third Order Dispersion of a Prismatic Pulse Compressor*”, Quantum Electronics 2000, Budapest, Hungary, paper 5 (2000).

[15] **P. Dombi**, A. Apolonski, G. G. Paulus, M. Kakehata, R. Holzwarth, Th. Udem, Ch. Lemell, J. Burgdörfer, T. W. Hänsch and F. Krausz, “*Solid-state light phase detector*” CLEO/QELS, Baltimore, Maryland, USA, Postdeadline paper QThPDA4 (2003).

[16] **P. Dombi**, A. Apolonski, G. G. Paulus, M. Kakehata, R. Holzwarth, Th. Udem, Ch. Lemell, J. Burgdörfer, T. W. Hänsch and F. Krausz, “*Lichtphasendetektor aus Festkörper*” 53. Jahrestagung der Österreichischen Physikalischen Gesellschaft, Salzburg, Austria, paper F-QEO03 (2003).

[17] Ch. Lemell, **P. Dombi**, X.-M. Tong, F. Krausz, J. Burgdörfer, „*Determination of the carrier-envelope phase of ultrashort laser pulses using metal surfaces*” 68. Physikertagung der Deutschen Physikalischen Gesellschaft, Munich, Germany, paper Q42.7 (2004).

[18] **P. Dombi**, F. Krausz, Gy. Farkas, “*Ultrafast dynamics of multiphoton photoemission and carrier-envelope phase sensitivity*”, Advanced Solid-State Photonics, Vienna, Austria (2005), accepted.

Other Publications

[19] I.N. Ross, C.J. Hooker, **P. Dombi**, „*A Grating Interferometer for the Recording of Large High Quality Gratings*”, Central Laser Facility, Annual Report 1999/2000, p.222-223 (Rutherford Appleton Laboratory, UK, 2000).

[20] K. Osvay, Z. Bor, **P. Dombi**, I.E. Ferincz, J. Hebling, A.P. Kovács, G. Kurdi, K. Varjú, “*TeWaTi – A versatile fs laser system with controllable chirp and tuneable UV pulses*”, First General Meeting of the ULTRA Programme of the European Science Foundation, Coimbra, Portugal, paper 34 (2000).

Publications relevant for this thesis: [3]-[7], [9], [11], [15]-[18]

Lebenslauf

Name:	Péter András DOMBI
Geburtstag/-ort:	19. Mai 1976 / Szeged (Ungarn)
Familienstand:	ledig
Staatsangehörigkeit:	Ungarn
Schulbildung:	1990-1994 Deák Ferenc Englisch–Ungarisches Zweisparchiges Gymnasium, Szeged
Berufsausbildung:	1994-2001 Physikstudium an der Universität Szeged mit zusätzlichem Lehramtsstudium 1995-2001 Religionspädagogikstudium an der Katholisch-Theologischen Hochschule Szeged
Stipendien, Preise:	1999, 2001 III. bzw. II. Preis auf der Landes- konferenz Ungarischer Studierenden, Sektion „Optik und Spektroskopie“ 2000-2001 Stipendium der Republik Ungarn
Abschluß:	Juni 2001 Mag.rer.nat.(Physik und Physik/Lehramt), Universität Szeged Juni 2001 Qualifikation in Religionsunterricht Katholisch-Theologische Hochschule
Berufstätigkeit:	Nov. 1998-Mai 2000 Forschungsmitarbeiter, Rutherford Appleton Laboratory, Central Laser Facility, Großbritannien. seit September 2001 Forschungsmitarbeiter an der Technischen Universität Wien, Institut für Photonik.
Sprachkenntnis:	Ungarisch (Muttersprache), Englisch, Deutsch (fließend), Spanisch, Französisch (Grundkenntnisse)
Veröffentlichungen:	8 Artikel in referierten wissenschaftlichen Zeitschriften, 9 Konferenzbeiträge, 2 sonstige Publikationen